

1 **A genome-wide association study of chronic ALT-based non-alcoholic**
2 **fatty liver disease in the Million Veteran Program with histological**
3 **and radiological validation**

4 Marijana Vujkovic^{1,2,*}, Shweta Ramdas^{3,*}, Kimberly M. Lorenz^{1,3,4}, Xiuqing Guo⁵, Rebecca
5 Darlay⁶, Heather J. Cordell⁶, Jing He⁷, Yevgeniy Gindin⁸, Chuhan Chung⁸, Rob P Meyers⁸, Carolin
6 V. Schneider³, Joseph Park^{3,2}, Kyung M. Lee⁹, Marina Serper¹, Rotonya M. Carr², David E.
7 Kaplan¹, Mary E. Haas¹⁰, Matthew T. MacLean³, Walter R. Witschey¹¹, Xiang
8 Zhu^{12,13,14,15}, Catherine Tcheandjieu^{12,16}, Rachel L. Kember^{17,18}, Henry R. Kranzler^{17,18}, Anurag
9 Verma^{1,3}, Ayush Giri¹⁹, Derek M. Klarin^{20,21,22}, Yan V. Sun^{23,24}, Jie Huang²⁵, Jennifer
10 Huffman²¹, Kate Townsend Creasy³, Nicholas J. Hand³, Ching-Ti Liu²⁶, Michelle T. Long²⁷, Jie
11 Yao⁵, Matthew Budoff²⁸, Jingyi Tan⁵, Xiaohui Li⁵, Henry J. Lin⁵, Yii-Der Ida Chen⁵, Kent D.
12 Taylor⁵, Ruey-Kang Chang⁵, Ronald M. Krauss²⁹, Silvia Vilarinho³⁰, Joseph Brancale³⁰, Jonas B.
13 Nielsen³¹, Adam E. Locke³¹, Marcus B. Jones³¹, Niek Verweij³¹, Aris Baras³¹, K. Rajender
14 Reddy², Brent A. Neuschwander-Tetri³², Jeffrey B. Schwimmer³³, Arun J. Sanyal³⁴, Naga
15 Chalasani³⁵, Katherine A. Ryan³⁶, Braxton D. Mitchell³⁷, Dipender Gill³⁸, Andrew D.
16 Wells^{39,40}, Elisabetta Manduchi⁴¹, Yedidya Saiman⁴², Nadim Mahmud⁴², Donald R.
17 Miller^{43,44}, Peter D. Reaven^{45,46}, Lawrence S. Phillips^{23,47}, Sumitra Muralidhar⁴⁸, Scott L.
18 DuVall^{9,49}, Jennifer S. Lee^{12,16}, Themistocles L. Assimes^{12,16}, Saiju Pyarajan^{21,50,51}, Kelly
19 Cho^{21,50}, Todd L. Edwards^{52,53}, Scott M. Damrauer^{1,54}, Peter W. Wilson^{23,55}, J. Michael
20 Gaziano^{21,50}, Christopher J. O'Donnell^{21,50,51}, Amit V. Khera^{20,22,51}, Struan F.A.
21 Grant^{56,40}, Christopher D. Brown³, Philip S. Tsao^{12,16}, Danish Saleheen^{57,58,59}, Luca A. Lotta³¹, Lisa

22 Bastarache⁷, Quentin M. Anstee⁶⁰, Ann K. Daly⁶¹, James B. Meigs^{22,51,62}, Jerome I. Rotter⁵, Julie
23 A. Lynch^{9,49,63}, Regeneron Genetics Center, DiscovEHR Collaboration, EPOS Consortium
24 Investigators, VA Million Veteran Program, Daniel J. Rader^{2,3,*}, Benjamin F.
25 Voight^{1,3,4,64,*}, Kyong-Mi Chang^{1,4,*}

26

27 *These authors contributed equally

28

29 Affiliations

30 ¹Corporal Michael J. Crescenz VA Medical Center, Philadelphia, PA, USA, ²Department of
31 Medicine, University of Pennsylvania Perelman School of Medicine, Philadelphia, PA,
32 USA, ³Department of Genetics, University of Pennsylvania Perelman School of Medicine,
33 Philadelphia, PA, USA, ⁴Department of Systems Pharmacology and Translational Therapeutics,
34 University of Pennsylvania Perelman School of Medicine, Philadelphia, PA, USA, ⁵The Institute for
35 Translational Genomics and Population Sciences, Department of Pediatrics, The Lundquist
36 Institute for Biomedical Innovation at Harbor-UCLA Medical Center, Torrance, CA,
37 USA, ⁶Population Health Sciences Institute, Newcastle University, Newcastle upon Tyne,
38 UK, ⁷Department of Biomedical Informatics, Vanderbilt University Medical Center, Nashville, TN,
39 USA, ⁸Bioinformatics and Clinical Data Science, Gilead Sciences, Inc., Foster City, CA, USA, ⁹VA
40 Salt Lake City Health Care System, Salt Lake City, UT, USA, ¹⁰Broad Institute of MIT and Harvard,
41 Cambridge, MA, USA, ¹¹Department of Radiology, University of Pennsylvania Perelman School of
42 Medicine, Philadelphia, PA, USA, ¹²VA Palo Alto Health Care System, Palo Alto, CA,
43 USA, ¹³Department of Statistics, The Pennsylvania State University, University Park, PA,
44 USA, ¹⁴Huck Institutes of the Life Sciences, The Pennsylvania State University, University Park, PA,
45 USA, ¹⁵Department of Statistics, Stanford University, Stanford, CA, USA, ¹⁶Department of
46 Medicine, Stanford University School of Medicine, Stanford, CA, USA, ¹⁷Mental Illness Research
47 Education and Clinical Center, Corporal Michael J. Crescenz VA Medical Center, Philadelphia, PA,
48 USA, ¹⁸Department of Psychiatry, University of Pennsylvania Perelman School of Medicine,
49 Philadelphia, PA, USA, ¹⁹Department of Obstetrics and Gynecology, Vanderbilt University Medical
50 Center, Nashville, TN, USA, ²⁰Center for Genomic Medicine, Massachusetts General Hospital,
51 Boston, MA, USA, ²¹VA Boston Healthcare System, Boston, MA, USA, ²²Program in Medical and
52 Population Genetics, Broad Institute of MIT and Harvard, Cambridge, MA, USA, ²³Atlanta VA
53 Medical Center, Decatur, GA, USA, ²⁴Department of Epidemiology, Emory University Rollins
54 School of Public Health, Atlanta, GA, USA, ²⁵Department of Global Health, School of Public
55 Health, Peking University, Beijing, China, ²⁶Department of Biostatistics, Boston University School

56 of Public Health, Boston, MA, USA, ²⁷Department of Medicine, Section of Gastroenterology,
57 Boston University School of Medicine, Boston, MA, USA, ²⁸Department of Cardiology, The
58 Lundquist Institute for Biomedical Innovation at Harbor-UCLA Medical Center, Torrance, CA,
59 USA, ²⁹Department of Medicine, Children's Hospital Oakland Research Institute, Oakland, CA,
60 USA, ³⁰Departments of Internal Medicine, Section of Digestive Diseases, and of Pathology, Yale
61 School of Medicine, New Haven, CT, USA, ³¹Regeneron Genetics Center, Tarrytown, NY,
62 USA, ³²Department of Internal Medicine, Saint Louis University, St. Louis, MO, USA, ³³Department
63 of Pediatrics, University of California San Diego, La Jolla, CA, USA, ³⁴Department of Internal
64 Medicine, Virginia Commonwealth University School of Medicine, Richmond, VA,
65 USA, ³⁵Department of Medicine, Indiana University School of Medicine, Indianapolis, IN,
66 USA, ³⁶VISN 5 Capitol Health Care Network Mental Illness Research Education and Clinical
67 Center, Baltimore, MD, USA, ³⁷Program for Personalized and Genomic Medicine, Division of
68 Endocrinology, Diabetes and Nutrition, Department of Medicine, University of Maryland School
69 of Medicine, Baltimore, MD, USA, ³⁸Department of Epidemiology and Biostatistics, School of
70 Public Health, Imperial College London, London, UK, ³⁹Department of Pathology and Laboratory
71 Medicine, University of Pennsylvania Perelman School of Medicine, Philadelphia, PA,
72 USA, ⁴⁰Division of Human Genetics, Children's Hospital of Philadelphia, Philadelphia, PA,
73 USA, ⁴¹Institute for Biomedical Informatics, University of Pennsylvania Perelman School of
74 Medicine, Philadelphia, PA, USA, ⁴²Department of Medicine, Division of Gastroenterology,
75 University of Pennsylvania Perelman School of Medicine, Philadelphia, PA, USA, ⁴³Edith Nourse
76 Rogers Memorial VA Hospital, Bedford, MA, USA, ⁴⁴Center for Population Health, University of
77 Massachusetts, Lowell, MA, USA, ⁴⁵Phoenix VA Health Care System, Phoenix, AZ, USA, ⁴⁶College of
78 Medicine, University of Arizona, Tuscon, AZ, USA, ⁴⁷Division of Endocrinology, Emory University
79 School of Medicine, Atlanta, GA, USA, ⁴⁸Office of Research and Development, Veterans Health
80 Administration, Washington, DC, USA, ⁴⁹Department of Medicine, University of Utah School of
81 Medicine, Salt Lake City, UT, USA, ⁵⁰Department of Medicine, Brigham Women's Hospital, Boston,
82 MA, USA, ⁵¹Department of Medicine, Harvard Medical School, Boston, MA, USA, ⁵²Nashville VA
83 Medical Center, Nashville, TN, USA, ⁵³Vanderbilt Genetics Institute, Vanderbilt University Medical
84 Center, Nashville, TN, USA, ⁵⁴Department of Surgery, University of Pennsylvania Perelman School
85 of Medicine, Philadelphia, PA, USA, ⁵⁵Division of Cardiology, Emory University School of
86 Medicine, Atlanta, GA, USA, ⁵⁶Department of Pediatrics, University of Pennsylvania Perelman
87 School of Medicine, Philadelphia, PA, USA, ⁵⁷Department of Medicine, Columbia University Irving
88 Medical Center, New York, NY, USA, ⁵⁸Department of Cardiology, Columbia University Irving
89 Medical Center, New York, NY, USA, ⁵⁹Center for Non-Communicable Diseases, Karachi, Sindh,
90 Pakistan, ⁶⁰Translational and Clinical Research Institute, Faculty of Medical Sciences, Newcastle
91 University, Newcastle upon Tyne, UK, ⁶¹Newcastle NIHR Biomedical Research Centre, Newcastle
92 upon Tyne Hospitals NHS Foundation Trust, Newcastle upon Tyne, UK, ⁶²Division of General
93 Internal Medicine, Massachusetts General Hospital, Boston, MA, USA, ⁶³College of Nursing and
94 Health Sciences, University of Massachusetts, Lowell, MA, USA, ⁶⁴Institute of Translational
95 Medicine and Therapeutics, University of Pennsylvania Perelman School of Medicine,
96 Philadelphia, PA, USA

97 **Abstract**

98 Nonalcoholic fatty liver disease (NAFLD) is a growing cause of chronic liver disease. Using a
99 proxy NAFLD definition of chronic alanine aminotransferase elevation (cALT) without other liver
100 diseases, we performed a trans-ancestry genome-wide association study in the Million Veteran
101 Program including 90,408 cALT cases and 128,187 controls. In the Discovery stage, seventy-
102 seven loci exceeded genome-wide significance – including 25 without prior NAFLD or ALT
103 associations – with one additional locus identified in European-only and two in African-
104 American-only analyses ($P < 5 \times 10^{-8}$). External replication in cohorts with NAFLD defined by
105 histology (7,397 cases, 56,785 controls) or liver fat extracted from radiologic imaging
106 ($n = 44,289$) validated 17 SNPs ($P < 6.5 \times 10^{-4}$) of which 9 were novel (*TRIB1*, *PPARG*, *MTTP*,
107 *SERPINA1*, *FTO*, *IL1RN*, *COBLL1*, *APOH*, and *IFI30*). Pleiotropy analysis showed that 61 of 77
108 trans-ancestry and all 17 validated SNPs were jointly associated with metabolic and/or
109 inflammatory traits, revealing a complex model of genetic architecture. Our approach
110 integrating cALT, histology and imaging reveals new insights into genetic liability to NAFLD.

111

112

113 **Introduction**

114 Chronic liver disease with progression to cirrhosis and hepatocellular carcinoma is a global
115 health issue¹. In particular, nonalcoholic fatty liver disease (NAFLD) – a hepatic phenotype
116 associated with metabolic syndrome and insulin resistance – is an increasingly common cause
117 of chronic liver disease with an estimated world prevalence of 25% among adults¹⁻⁵. In the
118 United States (US), NAFLD prevalence is projected to reach 33.5% among the adult population
119 by 2030, due in large part to rising rates of obesity and other cardiometabolic risk factors⁶.
120 NAFLD is defined by $\geq 5\%$ fat accumulation in the liver (hepatic steatosis) in the absence of other
121 known causes for liver disease, based on liver biopsy and/or non-invasive radiologic imaging^{3,4}.
122 The clinical spectrum of NAFLD ranges from bland steatosis to nonalcoholic steatohepatitis
123 (NASH) involving inflammation and hepatocellular ballooning injury with progressive fibrosis. At
124 least 20% of patients with NAFLD develop NASH with increased risk of consequent cirrhosis and
125 primary liver cancer^{5,6}. To date, there is no licensed drug approved to treat NAFLD and prevent
126 its progression, and the general therapeutic approach focuses on improving the underlying
127 metabolic disorders such as glucose control and promotion of weight loss.

128 Individual susceptibility to NAFLD involves both genetic and environmental risk factors.
129 Current estimates of NAFLD heritability range from 20% to 50%⁷ while risk factors for NAFLD
130 include obesity (in particular, abdominal adiposity), insulin resistance and several features of
131 metabolic syndrome^{2,5,6,8}. Several genetic variants that promote the full spectrum of fatty liver
132 disease have been identified in genome-wide association studies (GWAS) utilizing cohorts
133 based on liver biopsy, imaging, and/or isolated liver enzyme values⁹⁻²². The most prominent
134 variants include p.I148M in *PNPLA3* and p.E167K in *TM6SF2*, which increase NAFLD risk, and a

135 loss-of-function variant in *HSD17B13* that confers protection against NASH¹⁶. However, the
136 limited number of genetic associations in NAFLD contrasts with other cardiometabolic disorders
137 where hundreds of loci have been mapped to date, such as obesity^{23,24}, type 2 diabetes²⁵,
138 hypertension²⁶, and plasma lipids²⁷. This highlights the need for expanded discovery with larger
139 samples and greater population diversity, with further integration of functional genomics data
140 sets to potentially identify the effector genes²⁸.

141 The Million Veteran Program (MVP) is among the world's largest and most ancestrally
142 diverse biobanks²⁹. The availability of comprehensive, longitudinally collected Veterans Health
143 Administration (VA) electronic health records for US Veteran participants in the MVP also
144 makes it a promising resource for precision medicine. However, NAFLD is markedly
145 underdiagnosed clinically due to the invasive nature of the liver biopsy procedure, variable use
146 of imaging modalities and poor sensitivity of international diagnostic codes (ICD) for NAFLD^{4,30}.
147 The use of chronic elevation of serum alanine aminotransferase levels (cALT) as a proxy for
148 NAFLD was shown to improve specificity and positive predictive value in the NAFLD diagnostic
149 algorithm within the VA Corporate Data Warehouse³¹. Accordingly, we recently adapted and
150 validated a cALT-based proxy NAFLD phenotype to facilitate case identification in MVP²¹,
151 applying a rigorous exclusion of other conditions that are known to increase liver enzymes (e.g.,
152 viral hepatitis, alcoholic liver disease, autoimmune liver disease, and known hereditary liver
153 disease). Moreover, we showed that our cALT-based proxy NAFLD phenotype had a sensitivity
154 of 80%, a specificity of 89%, an accuracy of 85%, a positive predictive value of 89%, and an area-
155 under-the-curve of 87% compared to gold standard abdominal imaging, liver biopsy, and clinical
156 notes in a well-characterized sample of 178 patients in the VA healthcare system. In the current

157 study, we applied this cALT-based proxy NAFLD phenotype in MVP participants of 4 ancestral
158 groups³², and identified 90,408 NAFLD cases and 128,187 controls (**Figure 1**, and
159 **Supplementary Figure 1**).

160 Our aims are to: (i) perform a trans-ancestry genetic susceptibility analysis of the cALT-
161 based proxy NAFLD phenotype in MVP; (ii) replicate the lead SNPs in external NAFLD cohorts
162 with hepatic fat defined by liver histology or radiologic imaging; (iii) identify putative causal
163 genes at the lead loci by using an ensemble “variant-to-gene” mapping method that integrates
164 results from coding and functional genomic annotations, and quantitative trait loci (QTL); and (iv)
165 identify each lead locus’s genetic architecture by characterizing its phenotypic association
166 profile using data from the GWAS catalog, MVP LabWAS, and MRC IEU OpenGWAS database.

167

168 **Results**

169 ***An ancestry-diverse study population with a high prevalence of cardiometabolic traits***

170 Our study consisted of 90,408 cALT cases and 128,187 controls comprising four ancestral
171 groups, namely European Americans (EA, 75.1%), African Americans (AA, 17.1%), Hispanic-
172 Americans (HISP, 6.9%), and Asian-Americans (ASN, 0.9%, **Supplemental Table 1**,
173 **Supplemental Figure 1**). Consistent with the US Veteran population, MVP cases and controls
174 ($n=218,595$) were predominantly male (92.3%) with an average age of 64 years at study
175 enrollment (**Supplemental Table 1**). The prevalence of cirrhosis and advanced fibrosis in the
176 cALT cases ranged from 4.7% to 9.1%. With the exclusion of other known causes of liver disease
177 as described previously²¹, cases were enriched for metabolic disorders (type 2 diabetes,

178 hypertension, and dyslipidemia), suggesting a link between chronic ALT elevation and metabolic
179 risk factors.

180

181 ***Identification of trans-ancestry and ancestry-specific cALT-associated loci in MVP***

182 To identify genetic loci associated with cALT, we performed trans-ancestry genome-wide scan
183 by meta-analyzing summary statistics derived from each individual ancestry (**Methods** and
184 **Figure 1**). In the trans-ancestry scan, 77 independent sentinel SNPs met conventional genome-
185 wide significance ($P < 5 \times 10^{-8}$), of which 60 SNPs exceeded trans-ancestry genome-wide
186 significance ($P < 5 \times 10^{-9}$). Of the 77 SNPs, 52 were previously reported to be associated with ALT,
187 including 9 that were also associated with NAFLD (i.e., *PNPLA3*, *TM6SF2*, *HSD17B13*, *PPP1R3B*,
188 *MTARC1*, *ERLIN1*, *APOE*, *GPAM*, and *SLC30A10;LYPLAL1*; **Figure 2** and **Supplemental Table 2**)<sup>9-
189 12,14,16-22,33-35</sup>. Of the 25 newly identified loci, 14 were novel (*IL1RN*, *P2RX7*, *CASP8*, *MERTK*,
190 *TRPS1*, *OGFRL1*, *HLA*, *SMARCD2;DDX42*, *CRIM1*, *FLT1*, *DNAJC22*, *HKDC1*, *UHRF2*, *STAP2;MPND*),
191 whereas 11 have been associated with gamma-glutamyl transferase (GGT) and/or alkaline
192 phosphatase (ALP) levels³⁵.

193 In the ancestry-specific analyses, 55 loci in EAs, eight loci in AAs, and three in HISPs
194 exceeded conventional genome-wide significance ($P < 5 \times 10^{-8}$, **Supplemental Tables 3-5** and
195 **Supplemental Figures 2-4**), of which 1 EA SNP and 2 AA SNPs were not captured in the trans-
196 ancestry analysis. No variants among ASN subjects achieved genome-wide significance, likely
197 due to limited sample size (**Supplemental Figure 5**). Notably, the top two SNPs in the AA-only
198 scan (with the genes *GPT* and *ABCB4* nearby each SNP, respectively) showed stronger

199 associations than observed for *PNPLA3*. These two SNPs are polymorphic among AA's but
200 nearly monomorphic in all other populations.

201

202 ***Replication of cALT-associated loci in liver biopsy and radiologic imaging data***

203 To validate that our cALT-associated SNPs capture genetic susceptibility to NAFLD, we
204 assembled two external NAFLD cohorts, namely: (i) a **Liver Biopsy Cohort** consisting of 7,397
205 histologically characterized NAFLD cases and 56,785 population controls from various clinical
206 studies (**Supplemental Table 6-7**), and (ii) a **Liver Imaging Cohort** consisting of 44,289
207 participants with available radiologic liver imaging data and quantitative hepatic fat (qHF)
208 measurements (**Supplemental Table 8**). For each cohort, we performed a trans-ancestry lookup
209 of the 77 lead SNPs (**Methods**). In the Liver Biopsy Cohort, there was directional concordance
210 between effect estimates of biopsy-defined NAFLD in 66 of 77 SNPs (86%), including 15 SNPs
211 with a significant association (adjusted Bonferroni nominal $P < 6.5 \times 10^{-4}$), of which 8 have not
212 been reported in genome- or exome-wide association studies previously (e.g., *TRIB1*, *MTTP*,
213 *APOH*, *IFI30*, *COBLL1*, *SERPINA1*, *IL1RN*, and *FTO*)(**Supplemental Table 7**)¹². In the Liver Imaging
214 Cohort, there was directional concordance between effect estimates of qHF in 49 of 77 SNPs
215 (64%). Among these, 11 were significantly associated with qHF (adjusted Bonferroni nominal P
216 $< 6.5 \times 10^{-4}$, **Supplemental Table 8**) of which 6 were novel (e.g., *TRIB1*, *MTTP*, *APOH*, *IFI30*,
217 *COBLL1*, and *PPARG*). As observed in previous studies owing to its role in glycogen storage (and
218 associated impact on imaging), the *PPP1R3B* locus was significantly associated with qHF,
219 however in the opposite direction from cALT, and not associated with biopsy-proven
220 NAFLD^{12,36}. Collectively, 17 of 77 SNPs were validated in external histologic and/or radiologic

221 NAFLD, of which 9 were previously unreported, namely five in both biopsy and imaging cohorts
222 (*TRIB1*, *MTTP*, *APOH*, *IFI30*, and *COBLL1*), three in biopsy cohort alone (*FTO*, *SERPINA1*, and
223 *IL1RN*) and one in imaging cohort with a nominal significance in biopsy cohort (*PPARG*)
224 (**Supplemental Table 1**). An additional 24 SNPs were nominally associated ($P < 0.05$) with
225 directional concordance with histological and/or radiologic hepatic fat.

226

227 ***Genomic risk scores and histologically characterized NAFLD***

228 We next constructed genetic risk scores (GRSs) based on effect estimates from our cALT GWAS
229 SNPs in 4 independent liver biopsy cohorts to quantify the cumulative predictive power of our
230 77 sentinel variants (**Supplemental Table 9, Supplemental Figure 8**). A 77 SNP-based GRS was
231 predictive of NAFLD in the meta-analyzed liver biopsy cohorts (GRS-77, $P = 3.7 \times 10^{-28}$).
232 Stratification of GRS-77 into a GRS consisting of a set of 7 well-established NAFLD SNPs (GRS-7),
233 and a GRS consisting of 70 remaining SNPs (GRS-70) revealed significant independent capacity
234 to predict histologically characterized NAFLD (GRS-7, $P = 1.7 \times 10^{-13}$; GRS-70, $P = 1.7 \times 10^{-5}$),
235 further supporting the clinical relevance of our panel of SNPs derived from proxy NAFLD
236 phenotype.

237

238 ***cALT heritability and genetic correlations with other phenotypes***

239 To further characterize the architecture of our cALT phenotype and its relationship with other
240 traits, we estimated heritability and genetic correlations with other traits using linkage
241 disequilibrium (LD) score regression³⁷⁻³⁹ (**Methods**). The SNP-based liability-scaled heritability
242 was estimated at 16% (95% CI: 12-19, $P < 1 \times 10^{-6}$) in EA. Genetic correlation analysis between

243 NAFLD from the EA-only scan and 774 complex traits from LD Hub (**Methods**) identified a total
244 of 116 significant associations (adjusted Bonferroni nominal $P < 6.5 \times 10^{-5}$, **Supplemental Table**
245 **10**). These encompassed 78 cardiometabolic risk factors (67.2%) including measures of obesity
246 and adiposity, type 2 diabetes, hypertension, dyslipidemia, and coronary artery disease, which
247 is consistent with reports from observational studies correlating these traits to NAFLD⁴⁰.
248 Additional genetically correlated traits represented general health conditions (11.2%),
249 educational attainment and/or socio-economic status (12.0%) and other conditions such as
250 gastro-oesophageal reflux, osteoarthritis, gout, alcohol intake, smoking, ovary removal, and
251 urinary albumin-to-creatinine ratio (9.5%).

252

253 ***Identification of conditionally independent cALT-associated variants***

254 To discover additional conditionally independent cALT signals within the 77 genomic regions,
255 we performed a formal conditional analysis using stepwise regression on individual level data
256 for all single-ancestry sentinel variants (namely 51 EA, 8 AA, and 3 HISP genomic regions). We
257 detected a total of 29 conditionally independent SNPs ($P < 1 \times 10^{-5}$) flanking five known and 16
258 novel cALT loci in EA (**Supplemental Table 11**). In particular, the GPT locus showed the highest
259 degree of regional complexity with 4 conditionally independent SNPs, followed by AKNA with 3
260 conditionally independent SNPs. For one novel locus located on chromosome 12 between 121-
261 122Mb, the trans-ancestry lead variant (rs1626329) was located in *P2RX7*, whereas the lead
262 peak variant for EA mapped to *HNF1A* (rs1169292, **Figure 3**). Both variants are in strong LD
263 with distinct coding variants (*P2RX7*: rs1718119, Ala348Thr; *HNF1A*: rs1169288, Ile27Leu) and
264 are compelling candidate genes for metabolic liver disease. In AA, we observed a total of six

265 conditionally independent variants at three genomic regions, namely three variants at *GPT*, two
266 at *AKNA* and one at the *ABCB4* locus (**Supplemental Table 11**). No conditionally independent
267 variants were identified in Hispanics. Collectively, 35 additional variants were identified at 22
268 loci across multiple ancestries by formal conditional analysis.

269

270 ***Fine mapping to define potential causal variants in 95% credible sets***

271 To leverage the increased sample size and population diversity to improve fine-mapping
272 resolution, we computed statistically derived 95% credible sets using Wakefield's approximate
273 Bayes' factors⁴¹ using the trans-ancestry, EA, AA, and HISP summary statistics (**Supplemental**
274 **Table 12-15, Methods**). Trans-ancestry fine-mapping reduced the median 95% credible set size
275 from 9 in EA (with IQR 3 - 17) to 7.5 variants (IQR 2 - 13). A total of 11 distinct cALT associations
276 (e.g. *MTARC1*, *IL1RN*, *OGFRL1*, *PPP1R3B*, *SOX7;RP1L1;C8orf74*, *TRIB1*, *ERLIN1*, *TRIM5*,
277 *OSGIN1;MLYCD*, *TM6SF2* and *PNPLA3*) were resolved to a single SNP in the trans-ancestry meta-
278 regression, with an 4 additional loci suggesting single SNP sets from EA (n=2) and AA (n=2)
279 ancestry-specific scans.

280

281 ***Liver-specific enrichment of cALT heritability***

282 To ascertain the tissues contributing to the disease-association underlying cALT heritability, we
283 performed tissue-specific heritability analysis using stratified LD score regression. The strongest
284 associations were observed for genomic annotations surveyed in liver, hepatocytes, adipose,
285 and immune cell types among others (e.g., liver histone H3K36me3 and H3K4me1, adipose
286 nuclei H3K27ac, spleen TCR $\gamma\delta$, eosinophils in visceral fat; $P < 0.001$, **Supplemental Table 16**).

287 Medical subject heading (MeSH)-based analysis showed enrichment mainly in hepatocytes and
288 liver (False Discovery Rate (FDR) < 5%, **Supplemental Table 17**). Gene set analysis showed
289 strongest associations for liver and lipid-related traits (P-value < 1×10^{-6} , **Supplemental Table**
290 **18**). Enrichment analyses using publicly-available epigenomic data implemented in GREGOR
291 enrichment analysis (**Methods**) showed that most significant enrichments were observed for
292 active enhancer chromatin state in liver, epigenetic modification of histone H3 in hepatocytes
293 or liver-derived HepG2 cells (e.g. H3K27Ac, H3K9ac, H3K4me1, H3K4me3; adjusted Bonferroni
294 nominal P < 1.8×10^{-5} , **Supplemental Table 19 and 20**). These analyses additionally support the
295 hypothesis that our cALT GWAS captures multiple physiological mechanisms that contribute to
296 NAFLD heritability. Furthermore, DEPICT-based predicted gene function nominated 28 gene
297 candidates, including the known genes *PNPLA3* and *ERLIN1* (FDR < 5%, **Supplemental Table 21**),
298 as well as well-known cardiometabolic disease genes such as *PPARG*.

299

300 ***Coding variants in putative causal genes driving cALT associations***

301 There were six novel trans-ancestry loci for which the lead SNP is a coding missense variant
302 (**Supplementary Table 22**), namely Thr1412Asn in *CPS1*, Glu430Gln in *GPT*, Val112Phe in *TRIM5*,
303 Ala163Thr in *DNAJC22*, Glu366Lys in *SERPINA1* and Cys325Gly in *APOH*. To identify additional
304 coding variants that may drive the association between the lead SNPs and cALT risk, we
305 investigated predicted loss of function (pLoF) and missense variants in high LD to the identified
306 cALT lead variants ($r^2 > 0.7$ in each respective 1000 Genomes super-population, **Supplemental**
307 **Table 22**). Four previously described missense variants were replicated in the current study,
308 including Thr165Ala in *MTARC1*, Ile291Val in *ERLIN1*, Glu167Lys in *TM6SF2* and Ile148Met in

309 *PNPLA3*. Among novel loci, missense variants in high LD with lead variants included the genes
310 *CCDC18*, *MERTK*, *APOL3*, *PPARG*, *MTTP*, *MLXIPL*, *ABCB4*, *AKNA*, *GPAM*, *SH2B3*, *P2RX7*, *NYNRIN*,
311 *ANPEP*, *IFI30* and *MPV17L2*. Among the trans-ancestry coding missense variants, eleven were
312 predicted based on two methods (SIFT, PolyPhen-2) to have potentially deleterious and/or
313 damaging effects in protein function (**Supplementary Table 22**)^{42,43}. An AA-specific locus on
314 chromosome (rs115038698, chr7:87024718) was in high LD to a nearby missense variant
315 Ala934Thr in *ABCB4* (rs61730509, AFR $r^2=0.92$) with a predicted deleterious effect, where the T-
316 allele confers an increased risk of cALT ($\beta=0.617$, $P=1.8 \times 10^{-20}$). In summary, among our 77 trans-
317 ancestry loci, 24 prioritized a candidate gene based on a missense variant in high LD with the
318 lead SNP, including 5 novel loci with external validation (e.g., *SERPINA1*, *APOH*, *PPARG*, *MTTP*
319 and *IFI30;MPV17L2*).

320

321 ***Additional approaches to nominating putative causal genes***

322 *Co-localization analyses:* We performed colocalization analyses with gene expression and
323 splicing across 48 tissues measured by the GTEx project, and overlapped our lead SNPs with
324 histone quantitative trait locus (QTL) data from primary liver to identify cALT-associated
325 variants that are also associated with change in gene expression (eQTLs), splice isoforms
326 (sQTLs), or histone modifications (hQTLs, **Methods, Supplemental Table 23**). Across all tissues,
327 a total of 123 genes were prioritized, including 20 genes expressed in liver tissue (**Methods**).
328 For liver tissue alone, a total of eight variant-gene pairs were identified where the allele
329 associated with protection against cALT was also associated with reduced transcription levels.
330 Furthermore, sQTL analysis in GTEx v8 identified two genes in the liver (*HSD17B13* and *ANPEP*)

331 and 13 genes that were affected in at least two tissues (**Supplemental Table 24**). Finally, two of
332 our lead SNPs were in high LD ($r^2 > 0.8$) with variants that regulated H3K27ac levels in liver
333 tissue (hQTLs), namely *EFHD1* (hQTL SNPs rs2140773, rs7604422 in *EFHD1*) and *FADS2* loci
334 (hQTL rs174566 in *FADS2*)⁴⁴.

335 Assay for chromatin accessibility using liver-derived cells: We next mapped our cALT loci to
336 regions of open chromatin using ATAC-seq in three biologically-relevant liver-derived tissues
337 (human liver, liver cancer cell line [HepG2], and hepatocyte-like cells [HLC] derived from
338 pluripotent stem cells)⁴⁵. Additionally, we used promoter-focused Capture-C data to identify
339 those credible sets that physically interact with genes in two relevant cell types (HepG2 and
340 liver). For each credible set, we identified genes with significant interactions (CHiCAGO score >
341 5, **Methods**) that overlap with at least one lead variant (**Supplemental Table 25**). These
342 datasets are useful entry points for deciphering regulatory mechanisms involved in the
343 pathophysiology of NAFLD. Based on DEPICT gene prediction, coding variant linkage analysis,
344 and QTL colocalization (**Supplemental Tables 18-25**), 215 potentially relevant genes were
345 identified for the 77 loci. A protein-protein interaction (PPI) analysis revealed that among the
346 192 available proteins, 86 nodes were observed, with strong PPI enrichment ($P < 9.0 \times 10^{-8}$)
347 indicating that the protein network shows substantially more interactions than expected by
348 chance (**Supplemental Table 26 and Supplemental Figure 6**).

349

350 **Variant-to-Gene Ensembl Mapping Approach to nominate putative causal genes**

351 We developed an ensemble method for predicting the likely causal effector gene at 77 loci
352 based on 8 distinct gene-mapping analyses, including: SNP-gene overlap, DEPICT gene

353 prediction, coding variant linkage, colocalization with eQTL, sQTL and hQTL, promotor Capture-
354 C and/or ATAC-Seq peak overlap, and PPI network analysis. For each gene that resides in a
355 sentinel locus, the number of times that it was identified in the eight analyses was summarized
356 into a nomination score which reflects the cumulative evidence that the respective gene is the
357 causal effector gene in the region. This ensemble method for mapping variants to genes
358 resulted in the nomination of a single gene as the causal effector gene at 53 of 77 genomic loci.
359 At the remaining 24 loci, two loci lacked any data to support the nomination of a causal gene,
360 and at 22 loci two or more causal genes were nominated because they shared the maximum
361 nomination score (**Supplemental Table 27**). We highlighted 35 loci for which a causal gene was
362 prioritized by at least 3 sources of evidence (or 4 sources of evidence for coding variants) in
363 **Table 1**. These included 6 loci with co-localizing eQTLs in liver or adipose tissues and connection
364 to the predicted gene via Promoter CaptureC data (i.e., *EPHA2*, *IL1RN*, *SHROOM3*, *HKDC1*,
365 *PANX1*, *DHODH*;HP).

366 Gene expression of nominated genes in the Liver Single Cell Atlas: To confirm that the
367 nominated genes are involved in liver biology, we performed a gene expression lookup in single
368 cell RNA-Seq data from the Liver Single Cell Atlas⁴⁶. As a result, for 76 of 77 loci a gene was
369 nominated that was expressed in at least one liver cell type, with exception of the rs9668670
370 locus which nominated several keratin genes (*KRT84*;*KRT82*;*KRT74*)(**Supplemental Table 23**).

371

372 **Transcription factor analysis**

373 We observed that 14 nominated genes are transcription factors (TF) (**Supplemental Table 28**).

374 Using the DoRothEA data in OmniPath we identified that two of these TFs have several

375 downstream target genes that were also identified in our GWAS scan (**Methods**). Notably, the
376 CEBPA TF targets the downstream genes *PPARG*, *TRIB1*, *GPAM*, *FTO*, *IRS1*, *CRIM1*, *HP*, *TBC1D8*,
377 and *CPS1*, but also *NCEH1*, a gene in the vicinity of one of our associations that lacked a
378 nominated candidate gene. Similarly, HNF1A, the lead gene in the EA scan (and corresponding
379 to the trans-ancestry *P2RX7* locus) targets *SLC2A2*, *MTTP*, and *APOH*.

380

381 ***Pleiotropy and related-trait genetic architecture of lead cALT SNPs***

382 We next sought to identify additional traits that were associated with our 77 trans-ancestry
383 lead SNPs using four different approaches. First, a LabWAS of distinct clinical laboratory test
384 results⁴⁷ in MVP (**Methods**) yielded 304 significant SNP-trait associations (adjusted Bonferroni
385 nominal $P = 3.1 \times 10^{-5}$, **Supplemental Table 29, Supplemental Figure 7**). Second, a PheWAS
386 Analysis in UK Biobank data using SAIGE (**Methods**) identified various SNP-trait associations
387 that mapped to loci previously associated with liver and cardiometabolic traits, as well as
388 additional enriched association for gallstones, gout, arthritis, and hernias (adjusted Bonferroni
389 nominal $P < 4.6 \times 10^{-7}$, **Supplemental Table 30**). In particular, we examined all associations for
390 PheCode 571.5, “Other chronic nonalcoholic liver disease” which comprised 1,664 cases and
391 400,055 controls, which with a disease prevalence of 0.4% seems to be underreported. Still, of
392 the 73 variants with available data, 14 were both nominally associated and directionally
393 consistent with our scan (signed binomial test $P=3.4 \times 10^{-9}$), providing additional validation for
394 our scan (**Supplementary Table 31**). Third, a SNP lookup using the curated data in the MRC IEU
395 OpenGWAS project (**Supplemental Table 32**) identified 2,892 genome-wide significant SNP-trait
396 associations for trans-ancestry SNPs, with additional 283 SNP-trait associations for the ancestry-

397 specific lead SNPs. Finally, we performed cross-trait regional colocalization analyses of EA, AA,
398 and HISP lead loci with 36 other GWAS statistics of cardiometabolic and blood cell related traits
399 (**Methods**). This resulted in significant regional colocalization for 64 SNP-trait pairs in EA, 32
400 SNP-trait pairs in AA, and 12 SNP trait pairs in HISP (**Supplemental Table 33**).

401 Based on the four analyses described above, we selected all SNP-trait associations
402 relevant phenotypes to NAFLD biology and classified them as liver (e.g. ALT, ALP, AST, and GGT),
403 metabolic (e.g. HDL, LDL, and total cholesterol, triglycerides, BMI, glucose, and HbA1c), or
404 inflammatory traits (e.g., C-reactive protein, white blood cell count, lymphocyte count,
405 granulocytes, neutrophils, monocyte count, basophils, eosinophils, and myeloid white cells)
406 (**Supplemental Tables 29-33, Figure 4**). Across the trans-ancestry lead variants (n=77), ancestry-
407 specific (n=3), and secondary proximal associations (*HNF1A*, n=1), 17 SNPs showed association
408 with only liver traits (**Figure 4**). In contrast, 20 loci showed associations with both liver and
409 metabolic traits whereas 5 loci (*IL1RN*, *TMEM147*; *ATP4A* and *RORA*) showed associations with
410 both liver and inflammatory traits. Finally, 38 loci showed association with all three traits: liver
411 enzymes, cardiometabolic risk, and inflammation, including 14/17 loci that were externally
412 validated in Liver Biopsy and/or Imaging Cohorts (color-coded in red in **Figure 4**). Collectively,
413 our findings identify novel cALT-associated genetic loci with pleotropic effects that may impact
414 hepatic, metabolic and inflammatory traits.

415

416 **Discussion**

417 In this study, we describe the first of its kind multi-ancestry GWAS of cALT-based NAFLD, which
418 resulted in a total of 77 trans-ancestry loci, of which 25 have not been associated with NAFLD

419 or ALT before. We additionally identified three ancestry-specific loci, as well as 29 conditionally
420 independent SNPs in EAs and six in AAs. We assembled two external replication cohorts with
421 histologically confirmed NAFLD (7,397 NAFLD cases and 56,785 population controls) and
422 hepatic fat defined by imaging (n = 44,289), and validated the association of 17 SNPs with
423 NAFLD, of which nine are novel (*TRIB1*, *PPARG*, *MTTP*, *SERPINA1*, *FTO*, *IL1RN*, *COBLL1*, *APOH*,
424 and *IFI30*). Furthermore, a GRS based on novel SNPs alone was predictive of histologically
425 defined NAFLD.

426 Pleiotropy analysis allowed us to characterize the genetic architecture of NAFLD and
427 remarkably, all validated SNPs showed significant associations with metabolic risk factors
428 and/or inflammatory traits, the most common being plasma lipid-related, followed by glycemic
429 traits, hypertension, and cardiovascular disease. Our ensemble variant-to-gene mapping
430 method nominated a single causal effector gene at 53 genomic loci. We found that these genes
431 were highly expressed in one or more cell types in the liver and have prior biological
432 connections to liver metabolism, physiology, or disease, making this list compelling for further
433 interrogation. Collectively, our findings offer a comprehensive, expanded, and refined view of
434 the genetic contribution to cALT-based NAFLD with potential clinical, pathogenic, and
435 therapeutic relevance.

436 Our proxy NAFLD phenotype was based on chronic ALT elevation with the exclusion of
437 other known diagnoses of liver disease or causes of ALT elevation (e.g. viral hepatitis, alcoholic
438 liver disease, hemochromatosis), based on previous validation within VA population^{21,31}. In this
439 regard, several GWAS studies of liver enzyme levels have been reported, particularly of serum
440 ALT^{10,11,16,34,35}, but not all studies systematically excluded other causes of ALT elevation. For

441 example, Pazoki et al recently reported 230 loci related to ALT, of which 52 were also included
442 in our panel of 77 (67.5%) lead cALT loci^{34,35}. While our cALT approach was designed to enhance
443 the specificity of non-invasive NAFLD diagnosis^{21,31}, this overlap is not surprising given the high
444 prevalence of NAFLD in the general population. Furthermore, we noted that inflammatory traits
445 were associated with over half of the cALT-based NAFLD loci in our study. Indeed, while ALT can
446 be normal in persons with hepatic steatosis, we focused on chronic ALT elevation that
447 represents ongoing hepatocellular injury that can promote liver disease progression. For our
448 controls, we excluded individuals with mild ALT elevation and selected healthier ‘super-
449 controls’ to minimize potential phenotype misclassification (e.g. attributing cases as controls)
450 that can result in a bias towards the null.

451 The MVP is one of the world’s largest and most ancestrally diverse biobanks, of which
452 25% of the participants are of non-European ancestry, and this diversity enhanced the value of
453 this study. Utilizing data from multiple ancestries allowed us to narrow down putative causal
454 variants for NAFLD through trans-ancestry fine-mapping. Moreover, we identified 2 cALT-based
455 NAFLD loci specifically in AAs. For example, the lead SNP at the *ABCB4* locus (rs115038698) was
456 in high LD with the missense variant rs61730509 (Ala934Thr, AFR $r^2=0.92$) and had a very
457 potent effect (OR=1.87, CI=1.64-2.14, $P=1.8 \times 10^{-20}$). This variant is of low frequency in AA
458 (MAF=1.2%) but virtually absent in EA and ASN. *ABCB4*, also known as multidrug resistance
459 protein 3 (*MDR3*), is a compelling candidate gene, as it is involved in hepatocyte lipid transport
460 and has been previously implicated in cholestasis, gallbladder disease, and adult biliary
461 fibrosis/cirrhosis⁴⁸⁻⁵⁰.

462 Ultimately, the affirmative external validation of our lead cALT-based NAFLD loci in
463 NAFLD cohorts with liver biopsies and imaging supports the relevance of our proxy phenotype
464 for NAFLD. A total of 17 loci associated with cALT-based NAFLD were also significantly
465 associated with hepatic fat based on liver biopsy and/or radiological imaging. These included
466 loci previously associated with NAFLD or all-cause cirrhosis (e.g., *PNPLA3*, *TM6SF2*, *HSD17B13*,
467 *MTARC1*, *ERLIN1*, *GPAM*, and *APOE*), but also included several of the novel loci reported here
468 (e.g., *TRIB1*, *SERPINA1*, *MTTP*, *IL1RN*, *IFI30*, *COBLL1*, *APOH*, *FTO*, *PPP1R3B* and *PPARG*). For all
469 loci except *PPP1R3B*, we observed concordant directionality of effects between cALT and
470 hepatic fat. The apparent discrepancy in the *PPP1R3B* locus has been reported before¹² and
471 may represent diffuse attenuation on radiologic images due to hepatic accumulation of
472 glycogen^{36,51} rather than triglycerides⁵². These novel and validated genes make excellent gene
473 candidates for NAFLD.

474 A substantial fraction of our cALT-based NAFLD loci showed a shared genetic co-
475 architecture with metabolic traits (Figure 4). Several genes and liver-enriched transcription
476 factors involved in LDL and triglyceride pathways have been identified, such as the liver-biopsy
477 and/or imaging validated *TRIB1*, *FTO*^{53,54}, *COBLL1*^{55,56}, *MTTP*, *TM6SF2*, *PPARG*, *APOE*, and
478 *GPAM*⁵⁷⁻⁶⁰, but also the cALT-only associated variants in *MLXIPL*, *MLXIP*, *CEBPA*, *FADS2*, *APOH*,
479 *RORA*, and *HNF1A*. *TRIB1* presumably regulates VLDL secretion by promoting the degradation
480 carbohydrate-response element binding protein (ChREBP, encoded by *MLXIPL*), reducing
481 hepatic lipogenesis and limiting triglyceride availability for apolipoprotein B (apoB) lipidation.
482 Furthermore, *TRIB1* co-activates the transcription of *MTTP*, which encodes the microsomal
483 triglyceride transfer protein that loads lipids onto assembling VLDL particles and facilitates their

484 secretion by hepatocytes. Lomitapide, a small molecule inhibitor of *MTTP*, is approved as a
485 treatment for lowering LDL cholesterol in homozygous familial hypercholesterolemia⁶¹ and a
486 potential therapeutic target for NAFLD. *TRIB1* is also involved in the degradation of the key
487 hepatocyte transcription factor, CCAAT/enhancer-binding protein alpha (*CEBPA*)⁶², which
488 together with *HNF1A* (HNF1 Homeobox A), *RORα* (retinoic acid receptor-related orphan
489 receptor-α) and *MIR-122* are involved in a feedback loop of the the liver-enriched transcription
490 factor network to control hepatocyte differentiation⁶³. *RORα* is also a suppressor of
491 transcriptional activity of peroxisome proliferator-activated receptor γ (PPARγ)^{64,65}. *PPARG*,
492 encoding PPARγ, upregulates LDL-receptor-related protein 1 (*LRP1*), which facilitates the
493 hepatic uptake of triglyceride-rich lipoproteins via interaction with apolipoprotein E (apoE)^{66,67}.
494 *PPARG* is predominantly expressed in adipose tissue, and hepatic expression levels of *PPARG*
495 are significantly increased in patients with NAFLD⁶⁸. Large randomized controlled clinical trials
496 have reported that the *PPARG* agonists rosiglitazone and pioglitazone improve NAFLD-related
497 hepatic steatosis, hepatic inflammation, and fibrosis⁶⁹⁻⁷³. However, the treatment is frequently
498 accompanied with weight gain and fluid retention, limiting its application and potential long-
499 term drug adherence. *RORα* however, competes with PPARγ for binding to PPARγ target
500 promoters, and therapeutic strategies designed to modulate *RORα* activity in conjunction with
501 PPARγ may be beneficial for the treatment of NAFLD. ApoE and ApoH⁵⁷ play an important role
502 in the production and clearance of VLDL by facilitating the hepatic uptake of triglyceride-rich
503 lipoproteins⁷⁴⁻⁷⁷. ApoE deficiency is suggested to affect hepatic lipid deposition in dietary-
504 challenged murine models⁷⁸. Similarly, a Western high-fat cholesterol-rich diet accelerates the
505 formation of NASH with fibrosis in ApoE-deficient mice⁷⁹.

506 More than half of our cALT-based NAFLD loci had a significant association with at least
507 one inflammatory trait (**Figure 4**), consistent with the multiple-hit hypothesis of NAFLD⁸⁰. For
508 example, the transcription factor MafB regulates macrophage differentiation⁸¹ and genetic
509 variation in *MAFB* has been associated with hyperlipidemia and hypercholesterolemia²⁷. Mice
510 with macrophage-specific *Mafb*-deficiency are more susceptible to obesity and
511 atherosclerosis^{82,83}. *FADS1* and *FADS2* are markedly induced during monocyte to macrophage
512 differentiation, and it is hypothesized that they impact metabolic disease by balancing
513 proinflammatory and proresolving lipid mediators^{84,85}. Another interesting locus is *IL1RN*, which
514 in our study is associated with lower risk of cALT and liver-biopsy characterized NAFLD. GTEx
515 data shows heterogeneous directions of effect across various tissues, with the minor G-allele
516 being associated with increased *IL1RN* expression in liver but decreased expression in
517 subcutaneous adipose tissue. *IL1RN* encodes the anti-inflammatory cytokine interleukin-1
518 receptor antagonist (IL-1Ra) and is a natural inhibitor of IL-1 activity by blocking the binding of
519 IL-1 β to IL-1R, and is considered a potential therapeutic target for NAFLD treatment⁸⁶. IL-1 β has
520 been shown to lead to chronic low-grade inflammation⁸⁷⁻⁸⁹, insulin resistance and hepatic fat,
521 and promotes hepatic steatosis, inflammation and fibrosis^{90,91}. A study in mice has shown that
522 IL-1R-deficiency protects from liver fibrosis⁹², and the deletion of IL-1R reduces liver injury in
523 acute liver disease by blocking IL-1 driven autoinflammation⁹³. In two studies of patients with
524 diabetes, blockade of IL-1 signaling with Anakinra (a recombinant form of IL-1Ra) improved
525 glycemic control⁹⁴⁻⁹⁶. It remains to be investigated whether remodeling of the adipose tissue
526 inflammasome via IL-1 signaling blockade in obesity-associated NAFLD offers potential
527 therapeutic benefit. Other loci implicated with inflammatory traits include *RORA*^{97,98}, *IFI30*^{99,100},

528 *CD276*¹⁰¹⁻¹⁰³, *FCGR2A*¹⁰⁴, and *P2RX7*¹⁰⁵⁻¹⁰⁷. Interestingly, these inflammation-related genes and
529 pathways emerged from our cALT-based NAFLD GWAS despite the indirect assessment of our
530 phenotype, clearly implicating inflammation early in NAFLD.

531 Finally, *PANX1* and *MERTK* genes that are associated with liver traits only seem
532 particularly interesting. For *PANX1*, the directional concordance of effects between cALT and
533 *PANX1* gene expression in the liver suggests possible relevance as a therapeutic target. It has
534 been reported that the genetic deletion of Pannexin 1 (encoded by *PANX1*) has a protective
535 effect in a mouse model of acute and chronic liver disease^{108,109}, and our data demonstrate that
536 a SNP near *PANX1* was associated with reduced *PANX1* expression and reduced risk of NAFLD.
537 These data nominate *PANX1* as a therapeutic target for silencing in NAFLD treatment. For
538 MerTK, two missense variants (Arg466Lys and Ile518Val, $r^2=0.98$) were predicted to affect
539 protein function. MerTK signaling in hepatic macrophages was recently shown to mediate
540 hepatic stellate cell activation and promote hepatic fibrosis progression¹¹⁰. Variants in *MERTK*
541 were associated with liver fibrosis progression in HCV-infected patients¹¹¹, raising the possibility
542 for MerTK as a novel therapeutic target against fibrosis¹¹². We emphasize that functional
543 studies of our nominated causal genes are needed to demonstrate causal relevance, their
544 impact on hepatosteatosis, and ultimately to determine their underlying mechanisms.

545 In conclusion, we discovered 77 genomic loci associated with cALT-based NAFLD in a
546 large, ancestrally diverse cohort. Our cases of cALT-based NAFLD were excluded for other
547 known causes of liver disease or elevated ALT and, not surprisingly, were substantially enriched
548 for metabolic disorders. We replicated our findings in external cohorts with hepatic fat defined
549 by liver biopsy or radiologic imaging. The genetic architecture of the lead loci indicate a

550 predominant involvement of metabolic and inflammatory pathways. This study constitutes a
551 much-needed large-scale, multi-ancestry genetic resource that can be used to build genetic
552 prediction models, identify causal mechanisms, and understand biological pathways
553 contributing to NAFLD initiation and disease progression.
554

555 **Table 1a. Gene nominations at loci with strongest evidence for coding variants.**

SNP	Position	Gene	AA-Change	SIFT/PP2*	e/sQTL**	Other†	Pleiotropy‡
rs6541349	1:93787867	CCDC18	p.Leu1134Val	+/-	+	.	M
rs2642438	1:220970028	MTARC1	p.Thr165Ala	-/-	+(A)	+	M
rs11683409	2:112770134	MERTK	p.Arg466Lys	-/-	.	++	.
rs17036160	3:12329783	PPARG	p.Pro12Ala	-/-	+	++	M
rs17598226	4:100496891	MTTP	p.Ile128Thr	-/-	+	+	.
rs115038698	7:87024718	ABCB4	p.Ala934Thr	+/+	+	+	M,I
rs799165	7:73052057	MLXIPL	p.Gln241His	-/+	+	+	M,I
			p.Ala358Val	-/-	+	+	M,I
rs7041363	9:117146043	AKNA	p.Pro624Leu	+/-	+	+	M
rs10883451	10:101924418	ERLIN1	p.Ile291Val	-/-	.	++	M
rs4918722	10:113947040	GPAM	p.Ile43Val	-/-	+	++	M
rs11601507	11:5701074	TRIM5	p.Val112Phe	-/-	.	++	M,I
rs1626329	12:121622023	P2RX7	p.Ala348Thr	-/-	+	+	.
rs11621792	14:24871926	NYNRIN	p.Ala978Thr	-/-	+(L,A)	+	M,I
rs28929474	14:94844947	SERPINA1	p.Glu366Lys	-/+	.	+++	M,I
rs7168849	15:90346227	ANPEP	p.Ala311Val	-/-	+(L)	+	.
rs1801689	17:64210580	APOH	p.Cys325Gly	+/+	.	++	M,I
rs132665	22:36564170	APOL3	p.Ser39Arg	-/-	+(A)	+	.
rs738408	22:44324730	PNPLA3	p.Ile148Met	+/+	.	+++	M,I

556 Genes nominated with various sources of evidence are listed as follows.

557 *Prio to the slash symbol: '+' indicates 'deleterious' in SIFT and '-' otherwise. After slash symbol: '+'
 558 denotes probably damaging in Polyphen-2 and '-' otherwise.

559 ** The '+' indicates colocalization between NAFLD GWAS variant and GTEx QTL varint (COLOC
 560 PP4/(PP3+PP4) > 0.9). (L) denotes QTL effect in Liver, (A) denotes QTL in Adipose.

561 †Each '+' represent evidence from DEPICT, PPI data, or if the lead SNP is within the transcript; coding
 562 variants also include '+' from hQTLs/Capture-C evidence.

563 ‡Pleiotropy is limited to association with Metabolic (M) or Inflammatory (I) Traits

564

565

566 **Table 1b. Gene nominations at loci with strongest evidence for non-coding variants.**

SNP	Position	Gene	hQTL	CaptureC	e/sQTL**	Other [†]	Pleiotropy [‡]
rs36086195	1:16510894	EPHA2	.	+	+(L,A)	+	M
rs6734238	2:113841030	IL1RN	.	+	+(A)	++	I
rs10201587	2:202202791	CASP8	.	+	+	+	M
rs11683367	2:233510011	EFHD1	+	.	+(L)	+	.
rs61791108	3:170732742	SLC2A2	.	+	.	+++	M
rs7653249	3:136005792	PCCB	.	.	+	++	M,I
rs12500824	4:77416627	SHROOM3	.	+	+(L)	+	M
rs10433937	4:88230100	HSD17B13	.	.	+(L,A)	+	M,I
rs799165	7:73052057	BCL7B	.	+	+	+	M,I
rs687621	9:136137065	ABO	.	.	+	+	M,I
rs35199395	10:70983936	HKDC1	.	+	+(L,A)	+	M
rs174535	11:61551356	FADS2	+	.	+(A)	++	M,I
rs56175344	11:93864393	PANX1	.	.	+(L,A)	++	.
rs34123446	12:122511238	MLXIP	.	+	+	+	M,I
rs12149380	16:72043546	DHODH	.	+	+	+	M,I
		HP	.	+	+(A)	.	M,I
rs2727324	17:61922102	DDX42	.	+	+	+	M
		SMARCD2	.	.	+	+	M
rs5117	19:45418790	APOC1	.	.	+	++	M,I

567 Genes nominated with various sources of evidence are listed as follows.

568 *Prio to the slash symbol: '+' indicates 'deleterious' in SIFT and '-' otherwise. After slash symbol: '+'
569 denotes probably damaging in Polyphen-2 and '-' otherwise.

570 ** The '+' indicates colocalization between NAFLD GWAS variant and GTEx QTL varint (COLOC
571 PP4/(PP3+PP4) > 0.9). (L) denotes QTL effect in Liver, (A) denotes QTL in Adipose.

572 †Each '+' represent evidence from DEPICT, PPI data, or if the lead SNP is within the transcript; coding
573 variants also include '+' from hQTLs/Capture-C evidence.

574 ‡Pleiotropy is limited to association with Metabolic (M) or Inflammatory (I) Traits

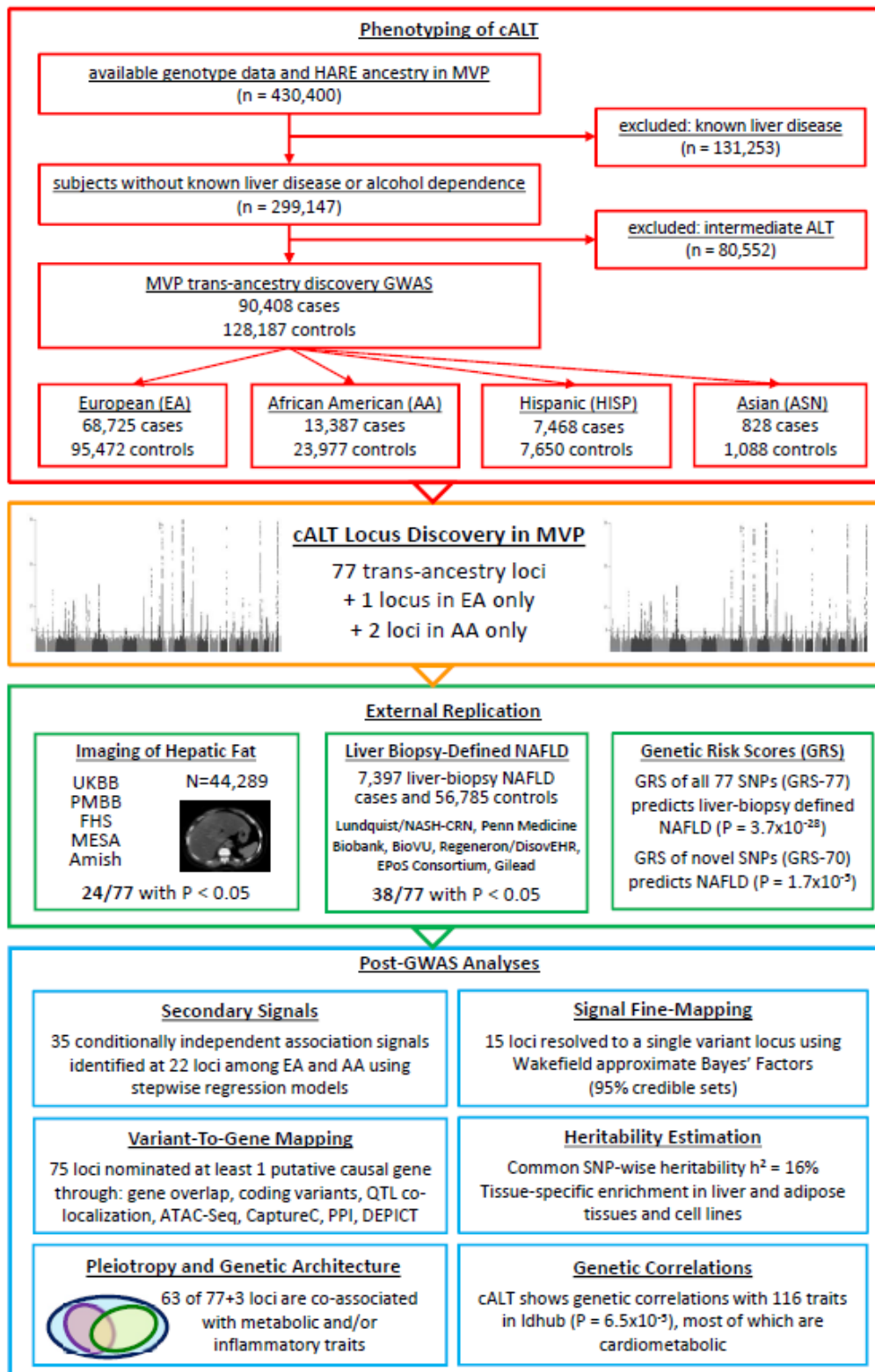
575

576

577

578

579 **Figure 1. Overview of analysis pipeline.**



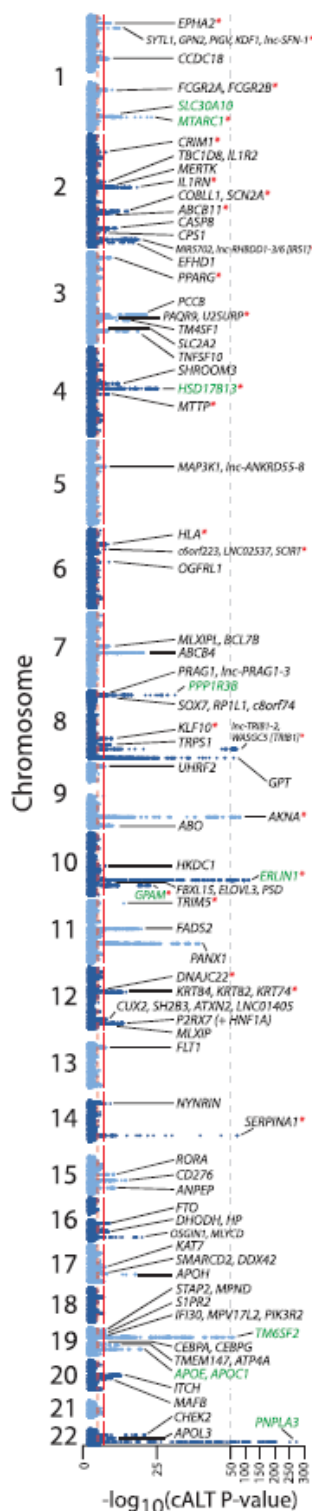
580

581 The flow diagram shows in the red box our study design with initial inclusion of 430,400 Million Veteran Program
582 participants with genotyping and ancestry classification by HARE, exclusion of individuals with known liver disease
583 or alcohol dependence and inclusion of subjects based on chronic ALT elevation (case) or normal ALT (control).
584 This resulted in 90,408 NAFLD cases and 128,187 controls with EA, AA, HISP and ASN ancestries that were
585 examined in primary trans-ancestry and ancestry-specific genome-wide association scans. The orange box of the
586 flow diagram highlights our results of trans-ancestry and ancestry-specific meta-analyses identifying 77 trans-
587 ancestry loci + 1 EA-specific + 2 AA-specific loci that met genome-wide significance. The green box summarizes the
588 results from external replication cohorts, whereas the blue box indicates all the post-GWAS annotation analyses
589 that we performed, which include secondary signal analysis, fine-mapping (95% credible sets), (tissue-specific)
590 heritability estimation, genetic correlations analysis, variant-to-gene mapping and pleiotropy analysis.

591

592

593 Figure 2. Manhattan plot of NAFLD GWAS of 90,408 NAFLD and 128, 187 controls in trans-
594 ancestry meta-analysis.



595

596 Nominated genes are indicated for 77 loci reaching genome-wide significance ($P < 5 \times 10^{-8}$).

597 Previously reported NAFLD-loci with genome-wide significant association are indicated in green

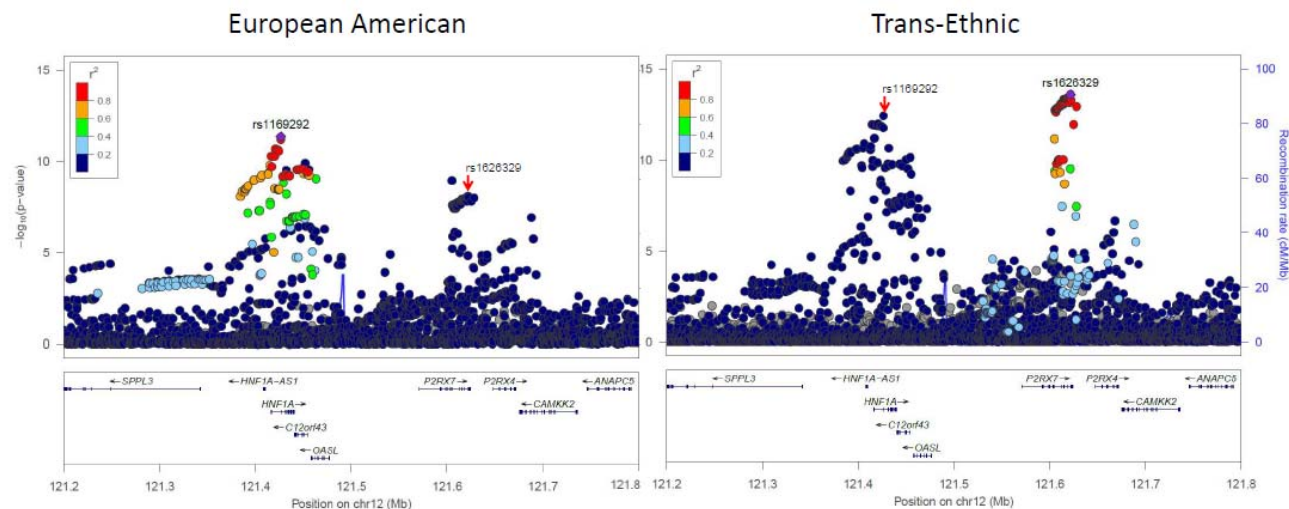
598 font. The red stars indicate the SNPs that have been validated with liver biopsy and/or

599 radiologic imaging.

600

601

602 **Figure 3. Chromosome 12 locus points to different genes in trans-ancestry (right) and**
603 **European-only (left) analyses.**

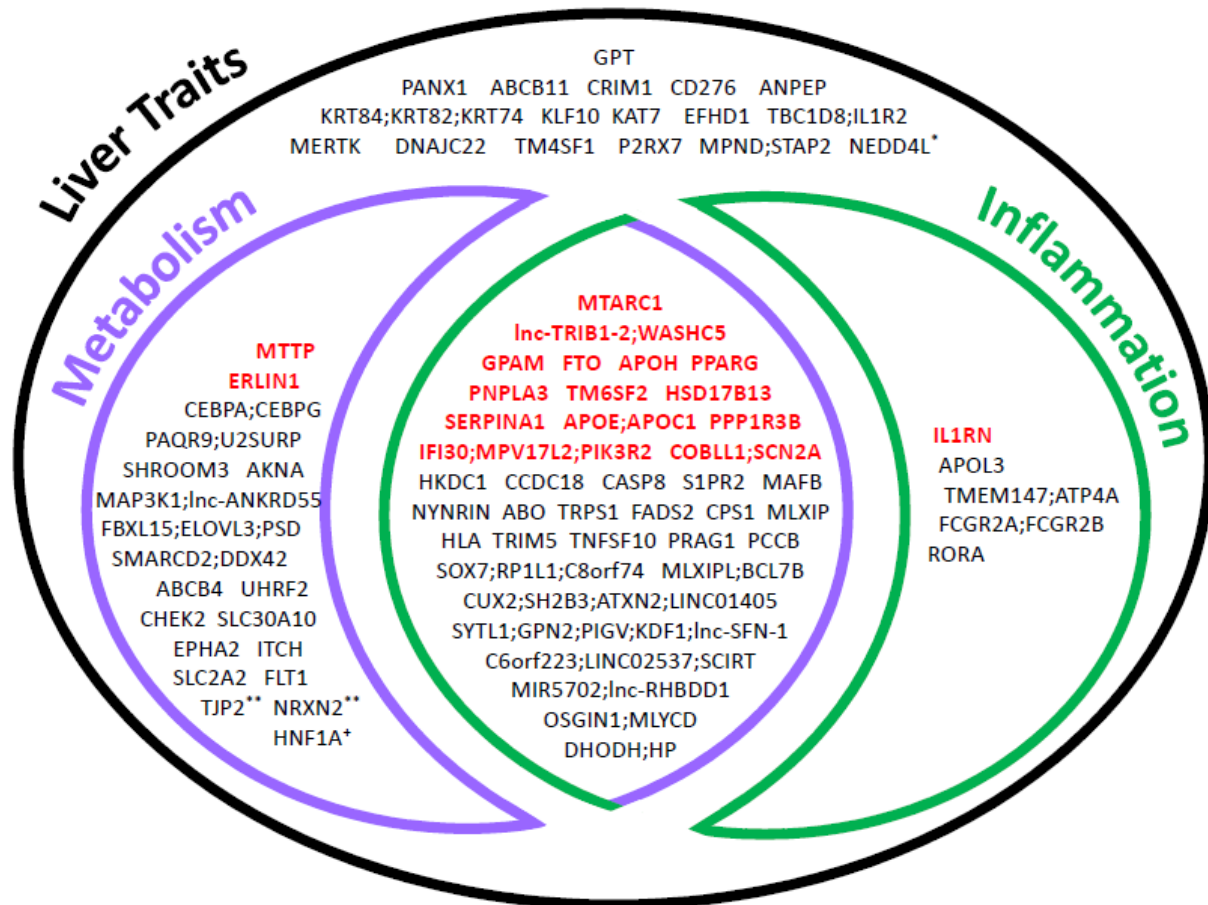


604
605 The lead variants in each analysis are highlighted (trans-ethnic on the right, european on the
606 left). The trans-ethnic peak concerns rs1626329 in P2RX7, whereas rs1169292 was identified in
607 European-only analysis and covers HNF1A. The r^2 between the two lead SNPs in < 0.01 in any of
608 the 1000 Genomes super-populations.

609

610

611 Figure 4. Venn diagram depicting overlapping liver, metabolic and inflammatory traits among
 612 NAFLD-associated loci.



613
 614 Overlapping liver (blackblack), metabolic (purplepurple) and/or inflammatory (green) traits are
 615 shown in association with 77 trans-ancestry and additional ancestry-specific lead SNPs. The trait
 616 categorizations reflect significant SNP-trait associations identified by: 1) LabWAS of clinical
 617 laboratory results in MVP; 2) PheWAS with UKBB data using SAIGE; 3) SNP lookup using the
 618 curated data in the IEU OpenGWAS projects; and 4) cross-trait colocalization analyses using
 619 COLOC of EA, AA and HISP lead loci with 36 other GWAS statistics of cardiometabolic and blood
 620 cell related traits. GenesGenes denoted in bold and color-coded in red refer to the loci also

621 associated with quantitative hepatic fat on imaging analyses or histologically characterized
622 NAFLD from liver biopsies. * Locus identified in European-only GWAS. ** Locus identified in
623 African American-restricted analysis. +Secondary signal from European analysis (e.g.
624 HNF1A/P2RX7).
625
626

627 **References**

- 628 1. Asrani, S.K., Devarbhavi, H., Eaton, J. & Kamath, P.S. Burden of liver diseases in the world. *J*
629 *Hepatol* **70**, 151-171 (2019).
- 630 2. Younossi, Z., Anstee, Q.M. & Marietti, M. Global burden of NAFLD and NASH: trends,
631 predictions, risk factors and prevention. *Nat Rev Gastroenterol Hepatol* **15**(2018).
- 632 3. Carr, R.M., Oranu, A. & Khungar, V. Nonalcoholic Fatty Liver Disease: Pathophysiology and
633 Management. *Gastroenterol Clin North Am* **45**, 639-652 (2016).
- 634 4. Chalasani, N. *et al.* The diagnosis and management of nonalcoholic fatty liver disease: Practice
635 guidance from the American Association for the Study of Liver Diseases. *Hepatology* **67**, 328-357
636 (2018).
- 637 5. Friedman, S.L., Neuschwander-Tetri, B.A., Rinella, M. & Sanyal, A.J. Mechanisms of NAFLD
638 development and therapeutic strategies. *Nat Med* **24**, 908-922 (2018).
- 639 6. Estes, C., Razavi, H., Loomba, R., Younossi, Z. & Sanyal, A.J. Modeling the epidemic of
640 nonalcoholic fatty liver disease demonstrates an exponential increase in burden of disease.
641 *Hepatology* **67**, 123-133 (2018).
- 642 7. Sookoian, S. & Pirola, C.J. Genetic predisposition in nonalcoholic fatty liver disease. *Clin Mol*
643 *Hepatol* **23**, 1-12 (2017).
- 644 8. Jarvis, H. *et al.* Metabolic risk factors and incident advanced liver disease in non-alcoholic fatty
645 liver disease (NAFLD): A systematic review and meta-analysis of population-based observational
646 studies. *PLoS Med* **17**, e1003100 (2020).
- 647 9. Romeo, S. *et al.* Genetic variation in PNPLA3 confers susceptibility to nonalcoholic fatty liver
648 disease. *Nat Genet* **40**, 1461-5 (2008).
- 649 10. Yuan, X. *et al.* Population-based genome-wide association studies reveal six loci influencing
650 plasma levels of liver enzymes. *Am J Hum Genet* **83**, 520-8 (2008).
- 651 11. Chambers, J.C. *et al.* Genome-wide association study identifies loci influencing concentrations of
652 liver enzymes in plasma. *Nat Genet* **43**, 1131-8 (2011).
- 653 12. Speliotes, E.K. *et al.* Genome-wide association analysis identifies variants associated with
654 nonalcoholic fatty liver disease that have distinct effects on metabolic traits. *PLoS Genet* **7**,
655 e1001324 (2011).
- 656 13. Feitosa, M.F. *et al.* The ERLIN1-CHUK-CWF19L1 gene cluster influences liver fat deposition and
657 hepatic inflammation in the NHLBI Family Heart Study. *Atherosclerosis* **228**, 175-80 (2013).
- 658 14. Kozlitina, J. *et al.* Exome-wide association study identifies a TM6SF2 variant that confers
659 susceptibility to nonalcoholic fatty liver disease. *Nat Genet* **46**, 352-6 (2014).
- 660 15. Liu, Y.L. *et al.* TM6SF2 rs58542926 influences hepatic fibrosis progression in patients with non-
661 alcoholic fatty liver disease. *Nat Commun* **5**, 4309 (2014).
- 662 16. Abul-Husn, N.S. *et al.* A Protein-Truncating HSD17B13 Variant and Protection from Chronic Liver
663 Disease. *N Engl J Med* **378**, 1096-1106 (2018).
- 664 17. Young, K.A. *et al.* Genome-Wide Association Study Identifies Loci for Liver Enzyme
665 Concentrations in Mexican Americans: The GUARDIAN Consortium. *Obesity (Silver Spring)* **27**,
666 1331-1337 (2019).
- 667 18. Namjou, B. *et al.* GWAS and enrichment analyses of non-alcoholic fatty liver disease identify
668 new trait-associated genes and pathways across eMERGE Network. *BMC Med* **17**, 135 (2019).
- 669 19. Emdin, C.A. *et al.* A missense variant in Mitochondrial Amidoxime Reducing Component 1 gene
670 and protection against liver disease. *PLoS Genet* **16**, e1008629 (2020).
- 671 20. Anstee, Q.M. *et al.* Genome-wide association study of non-alcoholic fatty liver and
672 steatohepatitis in a histologically characterised cohort(). *J Hepatol* **73**, 505-515 (2020).

- 673 21. Serper, M. *et al.* Validating a Non-Invasive Non-Alcoholic Fatty Liver Phenotype in the Million
674 Veteran Program. *PLoS One* (**in press**)(2020).
- 675 22. Chalasani, N. *et al.* Genome-wide association study identifies variants associated with histologic
676 features of nonalcoholic Fatty liver disease. *Gastroenterology* **139**, 1567-76, 1576 e1-6 (2010).
- 677 23. Locke, A.E. *et al.* Genetic studies of body mass index yield new insights for obesity biology.
678 *Nature* **518**, 197-206 (2015).
- 679 24. Yengo, L. *et al.* Meta-analysis of genome-wide association studies for height and body mass
680 index in approximately 700000 individuals of European ancestry. *Hum Mol Genet* **27**, 3641-3649
681 (2018).
- 682 25. Vujkovic, M. *et al.* Discovery of 318 new risk loci for type 2 diabetes and related vascular
683 outcomes among 1.4 million participants in a multi-ancestry meta-analysis. *Nat Genet* **52**, 680-
684 691 (2020).
- 685 26. Evangelou, E. *et al.* Genetic analysis of over 1 million people identifies 535 new loci associated
686 with blood pressure traits. *Nat Genet* **50**, 1412-1425 (2018).
- 687 27. Klarin, D. *et al.* Genetics of blood lipids among ~300,000 multi-ethnic participants of the Million
688 Veteran Program. *Nat Genet* **50**, 1514-1523 (2018).
- 689 28. Consortium, G.T. The Genotype-Tissue Expression (GTEx) project. *Nat Genet* **45**, 580-5 (2013).
- 690 29. Gaziano, J.M. *et al.* Million Veteran Program: A mega-biobank to study genetic influences on
691 health and disease. *J Clin Epidemiol* **70**, 214-23 (2016).
- 692 30. Hayward, K.L. *et al.* Detecting non-alcoholic fatty liver disease and risk factors in health
693 databases: accuracy and limitations of the ICD-10-AM. *BMJ Open Gastroenterol* **8**(2021).
- 694 31. Husain, N. *et al.* Nonalcoholic fatty liver disease (NAFLD) in the Veterans Administration
695 population: development and validation of an algorithm for NAFLD using automated data.
696 *Aliment Pharmacol Ther* **40**, 949-54 (2014).
- 697 32. Fang, H. *et al.* Harmonizing genetic ancestry and self-identified race/ethnicity in genome-wide
698 association studies. *Am J Hum Gen* **105**, 763-772 (2019).
- 699 33. de Vries, P.S. *et al.* Multiancestry Genome-Wide Association Study of Lipid Levels Incorporating
700 Gene-Alcohol Interactions. *Am J Epidemiol* **188**, 1033-1054 (2019).
- 701 34. Chen, V.L. *et al.* Genome-wide association study of serum liver enzymes implicates diverse
702 metabolic and liver pathology. *Nat Commun* **12**, 816 (2021).
- 703 35. Pazoki, R. *et al.* Genetic analysis in European ancestry individuals identifies 517 loci associated
704 with liver enzymes. *Nat Commun* (**in press**)(2021).
- 705 36. Stender, S. *et al.* Relationship between genetic variation at PPP1R3B and levels of liver glycogen
706 and triglyceride. *Hepatology* **67**, 2182-2195 (2018).
- 707 37. Finucane, H.K. *et al.* Partitioning heritability by functional annotation using genome-wide
708 association summary statistics. *Nat Genet* **47**, 1228-35 (2015).
- 709 38. Bulik-Sullivan, B.K. *et al.* LD Score regression distinguishes confounding from polygenicity in
710 genome-wide association studies. *Nat Genet* **47**, 291-5 (2015).
- 711 39. Finucane, H.K. *et al.* Heritability enrichment of specifically expressed genes identifies disease-
712 relevant tissues and cell types. *Nat Genet* **50**, 621-629 (2018).
- 713 40. Stephens, C.R. *et al.* The Impact of Education and Age on Metabolic Disorders. *Front Public*
714 *Health* **8**, 180 (2020).
- 715 41. Wakefield, J. Bayes factors for genome-wide association studies: comparison with P-values.
716 *Genet Epidemiol* **33**, 79-86 (2009).
- 717 42. Adzhubei, I., Jordan, D.M. & Sunyaev, S.R. Predicting functional effect of human missense
718 mutations using PolyPhen-2. *Curr Protoc Hum Genet* **Chapter 7**, Unit7 20 (2013).
- 719 43. Ng, M.C. *et al.* Meta-analysis of genome-wide association studies in African Americans provides
720 insights into the genetic architecture of type 2 diabetes. *PLoS Genet* **10**, e1004517 (2014).

- 721 44. Caliskan, M. *et al.* Genetic and Epigenetic Fine Mapping of Complex Trait Associated Loci in the
722 Human Liver. *Am J Hum Genet* **105**, 89-107 (2019).
- 723 45. Baxter, M. *et al.* Phenotypic and functional analyses show stem cell-derived hepatocyte-like cells
724 better mimic fetal rather than adult hepatocytes. *J Hepatol* **62**, 581-9 (2015).
- 725 46. Brancale, J. & Vilarinho, S. A single cell gene expression atlas of 28 human livers. *J Hepatol*
726 (2021).
- 727 47. Goldstein, J.A. *et al.* LabWAS: novel findings and study design recommendations from a meta-
728 analysis of clinical labs in two independent biobanks. *medRxiv*, 2020.04.08.19011478 (2020).
- 729 48. Sticova, E. & Jirsa, M. ABCB4 disease: Many faces of one gene deficiency. *Ann Hepatol* **19**, 126-
730 133 (2020).
- 731 49. Gudbjartsson, D.F. *et al.* Large-scale whole-genome sequencing of the Icelandic population. *Nat*
732 *Genet* **47**, 435-44 (2015).
- 733 50. Stattermayer, A.F., Halilbasic, E., Wrba, F., Ferenci, P. & Trauner, M. Variants in ABCB4 (MDR3)
734 across the spectrum of cholestatic liver diseases in adults. *J Hepatol* **73**, 651-663 (2020).
- 735 51. Dwyer, A. *et al.* Influence of glycogen on liver density: computed tomography from a metabolic
736 perspective. *J Comput Assist Tomogr* **7**, 70-3 (1983).
- 737 52. Mehta, M.B. *et al.* Hepatic protein phosphatase 1 regulatory subunit 3B (Ppp1r3b) promotes
738 hepatic glycogen synthesis and thereby regulates fasting energy homeostasis. *J Biol Chem* **292**,
739 10444-10454 (2017).
- 740 53. Wang, L. *et al.* NADP modulates RNA m(6)A methylation and adipogenesis via enhancing FTO
741 activity. *Nat Chem Biol* **16**, 1394-1402 (2020).
- 742 54. Wang, C.Y. *et al.* Loss of FTO in adipose tissue decreases Angptl4 translation and alters
743 triglyceride metabolism. *Sci Signal* **8**, ra127 (2015).
- 744 55. Chen, Z. *et al.* Functional Screening of Candidate Causal Genes for Insulin Resistance in Human
745 Preadipocytes and Adipocytes. *Circ Res* **126**, 330-346 (2020).
- 746 56. Nielsen, J.B. *et al.* Loss-of-function genomic variants highlight potential therapeutic targets for
747 cardiovascular disease. *Nat Commun* **11**, 6417 (2020).
- 748 57. Fagerberg, L. *et al.* Analysis of the human tissue-specific expression by genome-wide integration
749 of transcriptomics and antibody-based proteomics. *Mol Cell Proteomics* **13**, 397-406 (2014).
- 750 58. Duff, M.O. *et al.* Genome-wide identification of zero nucleotide recursive splicing in *Drosophila*.
751 *Nature* **521**, 376-9 (2015).
- 752 59. Jamialahmadi, O. *et al.* Exome-Wide Association Study on Alanine Aminotransferase Identifies
753 Sequence Variants in the GPAM and APOE Associated With Fatty Liver Disease.
754 *Gastroenterology* **160**, 1634-1646 e7 (2021).
- 755 60. Hammond, L.E. *et al.* Mitochondrial glycerol-3-phosphate acyltransferase-deficient mice have
756 reduced weight and liver triacylglycerol content and altered glycerolipid fatty acid composition.
757 *Mol Cell Biol* **22**, 8204-14 (2002).
- 758 61. Cuchel, M. *et al.* Inhibition of microsomal triglyceride transfer protein in familial
759 hypercholesterolemia. *N Engl J Med* **356**, 148-56 (2007).
- 760 62. Soubeyrand, S., Martinuk, A. & McPherson, R. TRIB1 is a positive regulator of hepatocyte nuclear
761 factor 4-alpha. *Sci Rep* **7**, 5574 (2017).
- 762 63. Laudadio, I. *et al.* A feedback loop between the liver-enriched transcription factor network and
763 miR-122 controls hepatocyte differentiation. *Gastroenterology* **142**, 119-29 (2012).
- 764 64. Kim, K. *et al.* RORalpha controls hepatic lipid homeostasis via negative regulation of
765 PPARgamma transcriptional network. *Nat Commun* **8**, 162 (2017).
- 766 65. Kim, J.Y., Han, Y.H., Nam, M.W., Kim, H.J. & Lee, M.O. RORalpha suppresses interleukin-6-
767 mediated hepatic acute phase response. *Sci Rep* **9**, 11798 (2019).

- 768 66. Laatsch, A. *et al.* Low density lipoprotein receptor-related protein 1 dependent endosomal
769 trapping and recycling of apolipoprotein E. *PLoS One* **7**, e29385 (2012).
- 770 67. Moon, J.H. *et al.* Upregulation of hepatic LRP1 by rosiglitazone: a possible novel mechanism of
771 the beneficial effect of thiazolidinediones on atherogenic dyslipidemia. *J Mol Endocrinol* **49**, 165-
772 74 (2012).
- 773 68. Skat-Rordam, J., Hojland Ipsen, D., Lykkesfeldt, J. & Tveden-Nyborg, P. A role of peroxisome
774 proliferator-activated receptor gamma in non-alcoholic fatty liver disease. *Basic Clin Pharmacol*
775 *Toxicol* **124**, 528-537 (2019).
- 776 69. Sanyal, A.J. *et al.* Pioglitazone, vitamin E, or placebo for nonalcoholic steatohepatitis. *N Engl J*
777 *Med* **362**, 1675-85 (2010).
- 778 70. Musso, G., Cassader, M., Paschetta, E. & Gambino, R. Thiazolidinediones and Advanced Liver
779 Fibrosis in Nonalcoholic Steatohepatitis: A Meta-analysis. *JAMA Intern Med* **177**, 633-640 (2017).
- 780 71. Ratziu, V. *et al.* Rosiglitazone for nonalcoholic steatohepatitis: one-year results of the
781 randomized placebo-controlled Fatty Liver Improvement with Rosiglitazone Therapy (FLIRT)
782 Trial. *Gastroenterology* **135**, 100-10 (2008).
- 783 72. Ratziu, V. *et al.* Long-term efficacy of rosiglitazone in nonalcoholic steatohepatitis: results of the
784 fatty liver improvement by rosiglitazone therapy (FLIRT 2) extension trial. *Hepatology* **51**, 445-53
785 (2010).
- 786 73. Cusi, K. *et al.* Long-Term Pioglitazone Treatment for Patients With Nonalcoholic Steatohepatitis
787 and Prediabetes or Type 2 Diabetes Mellitus: A Randomized Trial. *Ann Intern Med* **165**, 305-15
788 (2016).
- 789 74. Luc, G. *et al.* Distribution of apolipoprotein E between apo B- and non apo B-containing
790 lipoproteins according to apo E phenotype. *Atherosclerosis* **131**, 257-62 (1997).
- 791 75. Nakaya, Y., Schaefer, E.J. & Brewer, H.B., Jr. Activation of human post heparin lipoprotein lipase
792 by apolipoprotein H (beta 2-glycoprotein I). *Biochem Biophys Res Commun* **95**, 1168-72 (1980).
- 793 76. Lin, K.Y. *et al.* Evidence for inhibition of low density lipoprotein oxidation and cholesterol
794 accumulation by apolipoprotein H (beta2-glycoprotein I). *Life Sci* **69**, 707-19 (2001).
- 795 77. Mabile, L. *et al.* Secreted apolipoprotein E reduces macrophage-mediated LDL oxidation in an
796 isoform-dependent way. *J Cell Biochem* **90**, 766-76 (2003).
- 797 78. Karavia, E.A., Papachristou, D.J., Kotsikogianni, I., Giopanou, I. & Kypreos, K.E. Deficiency in
798 apolipoprotein E has a protective effect on diet-induced nonalcoholic fatty liver disease in mice.
799 *FEBS J* **278**, 3119-29 (2011).
- 800 79. Schierwagen, R. *et al.* Seven weeks of Western diet in apolipoprotein-E-deficient mice induce
801 metabolic syndrome and non-alcoholic steatohepatitis with liver fibrosis. *Sci Rep* **5**, 12931
802 (2015).
- 803 80. Tilg, H., Adolph, T.E. & Moschen, A.R. Multiple Parallel Hits Hypothesis in Nonalcoholic Fatty
804 Liver Disease: Revisited After a Decade. *Hepatology* **73**, 833-842 (2021).
- 805 81. Hamada, M., Tsunakawa, Y., Jeon, H., Yadav, M.K. & Takahashi, S. Role of MafB in macrophages.
806 *Exp Anim* **69**, 1-10 (2020).
- 807 82. Tran, M.T. *et al.* MafB deficiency accelerates the development of obesity in mice. *FEBS Open Bio*
808 **6**, 540-7 (2016).
- 809 83. Hamada, M. *et al.* MafB promotes atherosclerosis by inhibiting foam-cell apoptosis. *Nat*
810 *Commun* **5**, 3147 (2014).
- 811 84. Stoffel, W. *et al.* Obesity resistance and deregulation of lipogenesis in Delta6-fatty acid
812 desaturase (FADS2) deficiency. *EMBO Rep* **15**, 110-20 (2014).
- 813 85. Ecker, J. *et al.* Induction of fatty acid synthesis is a key requirement for phagocytic
814 differentiation of human monocytes. *Proc Natl Acad Sci U S A* **107**, 7817-22 (2010).

- 815 86. Mirea, A.M., Tack, C.J., Chavakis, T., Joosten, L.A.B. & Toonen, E.J.M. IL-1 Family Cytokine
816 Pathways Underlying NAFLD: Towards New Treatment Strategies. *Trends Mol Med* **24**, 458-471
817 (2018).
- 818 87. Hotamisligil, G.S. Inflammation and metabolic disorders. *Nature* **444**, 860-7 (2006).
- 819 88. Negrin, K.A. *et al.* IL-1 signaling in obesity-induced hepatic lipogenesis and steatosis. *PLoS One* **9**,
820 e107265 (2014).
- 821 89. Osborn, O. & Olefsky, J.M. The cellular and signaling networks linking the immune system and
822 metabolism in disease. *Nat Med* **18**, 363-74 (2012).
- 823 90. Tan, Q. *et al.* The Role of IL-1 Family Members and Kupffer Cells in Liver Regeneration. *Biomed*
824 *Res Int* **2016**, 6495793 (2016).
- 825 91. Gieling, R.G., Wallace, K. & Han, Y.P. Interleukin-1 participates in the progression from liver
826 injury to fibrosis. *Am J Physiol Gastrointest Liver Physiol* **296**, G1324-31 (2009).
- 827 92. Meier, R.P.H. *et al.* Interleukin-1 Receptor Antagonist Modulates Liver Inflammation and Fibrosis
828 in Mice in a Model-Dependent Manner. *Int J Mol Sci* **20**(2019).
- 829 93. Gehrke, N. *et al.* Hepatocyte-specific deletion of IL1-RI attenuates liver injury by blocking IL-1
830 driven autoinflammation. *J Hepatol* **68**, 986-995 (2018).
- 831 94. Larsen, C.M. *et al.* Interleukin-1-receptor antagonist in type 2 diabetes mellitus. *N Engl J Med*
832 **356**, 1517-26 (2007).
- 833 95. van Asseldonk, E.J. *et al.* One week treatment with the IL-1 receptor antagonist anakinra leads
834 to a sustained improvement in insulin sensitivity in insulin resistant patients with type 1
835 diabetes mellitus. *Clin Immunol* **160**, 155-62 (2015).
- 836 96. Banerjee, A. & Singh, J. Remodeling adipose tissue inflammasome for type 2 diabetes mellitus
837 treatment: Current perspective and translational strategies. *Bioeng Transl Med* **5**, e10150
838 (2020).
- 839 97. Han, Y.H. *et al.* A maresin 1/RORalpha/12-lipoxygenase autoregulatory circuit prevents
840 inflammation and progression of nonalcoholic steatohepatitis. *J Clin Invest* **129**, 1684-1698
841 (2019).
- 842 98. Chai, C. *et al.* Agonist of RORA Attenuates Nonalcoholic Fatty Liver Progression in Mice via Up-
843 regulation of MicroRNA 122. *Gastroenterology* **159**, 999-1014 e9 (2020).
- 844 99. West, L.C. & Cresswell, P. Expanding roles for GILT in immunity. *Curr Opin Immunol* **25**, 103-8
845 (2013).
- 846 100. Chiang, H.S. & Maric, M. Lysosomal thiol reductase negatively regulates autophagy by altering
847 glutathione synthesis and oxidation. *Free Radic Biol Med* **51**, 688-99 (2011).
- 848 101. Chapoval, A.I. *et al.* B7-H3: a costimulatory molecule for T cell activation and IFN-gamma
849 production. *Nat Immunol* **2**, 269-74 (2001).
- 850 102. Sun, T.W. *et al.* B7-H3 is expressed in human hepatocellular carcinoma and is associated with
851 tumor aggressiveness and postoperative recurrence. *Cancer Immunol Immunother* **61**, 2171-82
852 (2012).
- 853 103. Kang, F.B. *et al.* B7-H3 promotes aggression and invasion of hepatocellular carcinoma by
854 targeting epithelial-to-mesenchymal transition via JAK2/STAT3/Slug signaling pathway. *Cancer*
855 *Cell Int* **15**, 45 (2015).
- 856 104. Li, L. *et al.* Identification of key genes in nonalcoholic fatty liver disease progression based on
857 bioinformatics analysis. *Mol Med Rep* **17**, 7708-7720 (2018).
- 858 105. Baeza-Raja, B. *et al.* Pharmacological inhibition of P2RX7 ameliorates liver injury by reducing
859 inflammation and fibrosis. *PLoS One* **15**, e0234038 (2020).
- 860 106. Di Virgilio, F., Dal Ben, D., Sarti, A.C., Giuliani, A.L. & Falzoni, S. The P2X7 Receptor in Infection
861 and Inflammation. *Immunity* **47**, 15-31 (2017).

- 862 107. Giuliani, A.L., Sarti, A.C., Falzoni, S. & Di Virgilio, F. The P2X7 Receptor-Interleukin-1 Liaison.
863 *Front Pharmacol* **8**, 123 (2017).
- 864 108. Willebrords, J. *et al.* Protective effect of genetic deletion of pannexin1 in experimental mouse
865 models of acute and chronic liver disease. *Biochim Biophys Acta Mol Basis Dis* **1864**, 819-830
866 (2018).
- 867 109. Cooreman, A. *et al.* Connexin and Pannexin (Hemi)Channels: Emerging Targets in the Treatment
868 of Liver Disease. *Hepatology* **69**, 1317-1323 (2019).
- 869 110. Cai, B. *et al.* Macrophage MerTK Promotes Liver Fibrosis in Nonalcoholic Steatohepatitis. *Cell*
870 *Metab* **31**, 406-421 e7 (2020).
- 871 111. Patin, E. *et al.* Genome-wide association study identifies variants associated with progression of
872 liver fibrosis from HCV infection. *Gastroenterology* **143**, 1244-1252 e12 (2012).
- 873 112. Wen, Y. & Ju, C. MerTK - A Novel Potential Target to Treat NASH Fibrosis. *Hepatology* (2020).
- 874 113. Hunter-Zinck, H. *et al.* Genotyping Array Design and Data Quality Control in the Million Veteran
875 Program. *Am J Hum Genet* **106**, 535-548 (2020).
- 876 114. Kranzler, H.R. *et al.* Genome-wide association study of alcohol consumption and use disorder in
877 274,424 individuals from multiple populations. *Nat Commun* **10**, 1499 (2019).
- 878 115. Justice, A.C. *et al.* AUDIT-C and ICD codes as phenotypes for harmful alcohol use: association
879 with ADH1B polymorphisms in two US populations. *Addiction* **113**, 2214-2224 (2018).
- 880 116. Chang, C.C. *et al.* Second-generation PLINK: rising to the challenge of larger and richer datasets.
881 *Gigascience* **4**, 7 (2015).
- 882 117. Willer, C.J., Li, Y. & Abecasis, G.R. METAL: fast and efficient meta-analysis of genomewide
883 association scans. *Bioinformatics* **26**, 2190-1 (2010).
- 884 118. Hutchinson, A., Watson, H. & Wallace, C. Correcting the coverage of credible sets in Bayesian
885 genetic fine-mapping. *bioRxiv*, 781062 (2019).
- 886 119. Haas, M.E. *et al.* Machine learning enables new insights into clinical significance of and genetic
887 contributions to liver fat accumulation. *medRxiv*, 2020.09.03.20187195 (2020).
- 888 120. MacLean, M.T. *et al.* Linking abdominal imaging traits to electronic health record phenotypes.
889 *medRxiv*, 2020.09.08.20190330 (2020).
- 890 121. Wattacheril, J. *et al.* Genome-Wide Associations Related to Hepatic Histology in Nonalcoholic
891 Fatty Liver Disease in Hispanic Boys. *J Pediatr* **190**, 100-107 e2 (2017).
- 892 122. Patton, H.M. *et al.* Clinical correlates of histopathology in pediatric nonalcoholic steatohepatitis.
893 *Gastroenterology* **135**, 1961-1971 e2 (2008).
- 894 123. Kleiner, D.E. *et al.* Design and validation of a histological scoring system for nonalcoholic fatty
895 liver disease. *Hepatology* **41**, 1313-21 (2005).
- 896 124. Lin, H.J. *et al.* Home use of a compact, 12lead ECG recording system for newborns. *J*
897 *Electrocardiol* **53**, 89-94 (2019).
- 898 125. Weinshilboum, R.M. & Wang, L. Pharmacogenomics: Precision Medicine and Drug Response.
899 *Mayo Clin Proc* **92**, 1711-1722 (2017).
- 900 126. Gawrieh, S. *et al.* A Pilot Genome-Wide Analysis Study Identifies Loci Associated With Response
901 to Obeticholic Acid in Patients With NASH. *Hepatol Commun* **3**, 1571-1584 (2019).
- 902 127. Simon, J.A. *et al.* Phenotypic predictors of response to simvastatin therapy among African-
903 Americans and Caucasians: the Cholesterol and Pharmacogenetics (CAP) Study. *Am J Cardiol* **97**,
904 843-50 (2006).
- 905 128. Hardy, T. *et al.* The European NAFLD Registry: A real-world longitudinal cohort study of
906 nonalcoholic fatty liver disease. *Contemp Clin Trials* **98**, 106175 (2020).
- 907 129. Dewey, F.E. *et al.* Distribution and clinical impact of functional variants in 50,726 whole-exome
908 sequences from the DiscovEHR study. *Science* **354**(2016).

- 909 130. Harrison, S.A. *et al.* Selonsertib for patients with bridging fibrosis or compensated cirrhosis due
910 to NASH: Results from randomized phase III STELLAR trials. *J Hepatol* **73**, 26-39 (2020).
- 911 131. Roden, D.M. *et al.* Development of a large-scale de-identified DNA biobank to enable
912 personalized medicine. *Clin Pharmacol Ther* **84**, 362-9 (2008).
- 913 132. Bulik-Sullivan, B. *et al.* An atlas of genetic correlations across human diseases and traits. *Nat*
914 *Genet* **47**, 1236-41 (2015).
- 915 133. Consortium, E.P. An integrated encyclopedia of DNA elements in the human genome. *Nature*
916 **489**, 57-74 (2012).
- 917 134. Roadmap Epigenomics, C. *et al.* Integrative analysis of 111 reference human epigenomes.
918 *Nature* **518**, 317-30 (2015).
- 919 135. Andersson, R. *et al.* An atlas of active enhancers across human cell types and tissues. *Nature*
920 **507**, 455-461 (2014).
- 921 136. Fehrmann, R.S. *et al.* Gene expression analysis identifies global gene dosage sensitivity in cancer.
922 *Nat Genet* **47**, 115-25 (2015).
- 923 137. Cahoy, J.D. *et al.* A transcriptome database for astrocytes, neurons, and oligodendrocytes: a new
924 resource for understanding brain development and function. *J Neurosci* **28**, 264-78 (2008).
- 925 138. Heng, T.S., Painter, M.W. & Immunological Genome Project, C. The Immunological Genome
926 Project: networks of gene expression in immune cells. *Nat Immunol* **9**, 1091-4 (2008).
- 927 139. Pers, T.H. *et al.* Biological interpretation of genome-wide association studies using predicted
928 gene functions. *Nat Commun* **6**, 5890 (2015).
- 929 140. Schmidt, E.M. *et al.* GREGOR: evaluating global enrichment of trait-associated variants in
930 epigenomic features using a systematic, data-driven approach. *Bioinformatics* **31**, 2601-6 (2015).
- 931 141. McLaren, W. *et al.* The Ensembl Variant Effect Predictor. *Genome Biol* **17**, 122 (2016).
- 932 142. Genomes Project, C. *et al.* A global reference for human genetic variation. *Nature* **526**, 68-74
933 (2015).
- 934 143. Chesi, A. *et al.* Genome-scale Capture C promoter interactions implicate effector genes at GWAS
935 loci for bone mineral density. *Nat Commun* **10**, 1260 (2019).
- 936 144. Pashos, E.E. *et al.* Large, Diverse Population Cohorts of hiPSCs and Derived Hepatocyte-like Cells
937 Reveal Functional Genetic Variation at Blood Lipid-Associated Loci. *Cell Stem Cell* **20**, 558-570
938 e10 (2017).
- 939 145. Wingett, S. *et al.* HiCUP: pipeline for mapping and processing Hi-C data. *F1000Res* **4**, 1310
940 (2015).
- 941 146. Cairns, J. *et al.* CHiCAGO: robust detection of DNA looping interactions in Capture Hi-C data.
942 *Genome Biol* **17**, 127 (2016).
- 943 147. Szklarczyk, D. *et al.* STRING v11: protein-protein association networks with increased coverage,
944 supporting functional discovery in genome-wide experimental datasets. *Nucleic Acids Res* **47**,
945 D607-D613 (2019).
- 946 148. Gagliano Taliun, S.A. *et al.* Exploring and visualizing large-scale genetic associations by using
947 PheWeb. *Nat Genet* **52**, 550-552 (2020).
- 948 149. Denny, J.C. *et al.* PheWAS: demonstrating the feasibility of a phenome-wide scan to discover
949 gene-disease associations. *Bioinformatics* **26**, 1205-10 (2010).
- 950 150. Loh, P.R. *et al.* Reference-based phasing using the Haplotype Reference Consortium panel. *Nat*
951 *Genet* **48**, 1443-1448 (2016).
- 952 151. Zhou, W. *et al.* Efficiently controlling for case-control imbalance and sample relatedness in large-
953 scale genetic association studies. *Nat Genet* **50**, 1335-1341 (2018).
- 954 152. Elsworth, B. *et al.* The MRC IEU OpenGWAS data infrastructure. *bioRxiv*, 2020.08.10.244293
955 (2020).

- 956 153. Shin, S.Y. *et al.* An atlas of genetic influences on human blood metabolites. *Nat Genet* **46**, 543-
957 550 (2014).
- 958 154. Kettunen, J. *et al.* Genome-wide study for circulating metabolites identifies 62 loci and reveals
959 novel systemic effects of LPA. *Nat Commun* **7**, 11122 (2016).
- 960 155. Hemani, G. *et al.* The MR-Base platform supports systematic causal inference across the human
961 phenome. *Elife* **7**(2018).
- 962 156. Sun, B.B. *et al.* Genomic atlas of the human plasma proteome. *Nature* **558**, 73-79 (2018).
- 963 157. Giambartolomei, C. *et al.* Bayesian test for colocalisation between pairs of genetic association
964 studies using summary statistics. *PLoS Genet* **10**, e1004383 (2014).
- 965 158. Giri, A. *et al.* Trans-ethnic association study of blood pressure determinants in over 750,000
966 individuals. *Nat Genet* **51**, 51-62 (2019).
- 967 159. Pulit, S.L. *et al.* Meta-analysis of genome-wide association studies for body fat distribution in
968 694 649 individuals of European ancestry. *Hum Mol Genet* **28**, 166-174 (2019).
- 969 160. Teumer, A. *et al.* Genome-wide association meta-analyses and fine-mapping elucidate pathways
970 influencing albuminuria. *Nat Commun* **10**, 4130 (2019).
- 971 161. Tin, A. *et al.* Target genes, variants, tissues and transcriptional pathways influencing human
972 serum urate levels. *Nat Genet* **51**, 1459-1474 (2019).
- 973 162. Wuttke, M. *et al.* A catalog of genetic loci associated with kidney function from analyses of a
974 million individuals. *Nat Genet* **51**, 957-972 (2019).
- 975 163. Astle, W.J. *et al.* The Allelic Landscape of Human Blood Cell Trait Variation and Links to Common
976 Complex Disease. *Cell* **167**, 1415-1429 e19 (2016).
- 977 164. Guo, H. *et al.* Integration of disease association and eQTL data using a Bayesian colocalisation
978 approach highlights six candidate causal genes in immune-mediated diseases. *Hum Mol Genet*
979 **24**, 3305-13 (2015).
- 980 165. Lambert, S.A. *et al.* The Human Transcription Factors. *Cell* **175**, 598-599 (2018).
- 981 166. Garcia-Alonso, L., Holland, C.H., Ibrahim, M.M., Turei, D. & Saez-Rodriguez, J. Benchmark and
982 integration of resources for the estimation of human transcription factor activities. *Genome Res*
983 **29**, 1363-1375 (2019).
- 984 167. Turei, D., Korcsmaros, T. & Saez-Rodriguez, J. OmniPath: guidelines and gateway for literature-
985 curated signaling pathway resources. *Nat Methods* **13**, 966-967 (2016).
- 986 168. Ceccarelli, F., Turei, D., Gabor, A. & Saez-Rodriguez, J. Bringing data from curated pathway
987 resources to Cytoscape with OmniPath. *Bioinformatics* **36**, 2632-2633 (2020).
- 988
- 989

990 **Methods**

991 We performed a large-scale trans-ancestry NAFLD GWAS in the Million Veteran Program. We
992 subsequently conducted analyses to facilitate the prioritization of these individual findings,
993 including transcriptome-wide predicted gene expression, secondary signal analysis, coding
994 variant mapping, variant-to-gene mapping, and pleiotropy analysis to fine-map the genomic loci
995 to putatively causal genes and biological mechanisms.

996

997 *Discovery cohort in Million Veteran Program.*

998 The Million Veteran Program (MVP) is a mega-biobank that was launched in 2011 and
999 supported entirely by the Veterans Health Administration (VA) Office of Research and
1000 Development in the United States (US) of America, to develop a genetic repository of US
1001 Veterans with additional information through the VA electronic health record system and MVP
1002 questionnaires to learn how genes, lifestyle and military exposure affect health and disease.
1003 The MVP received ethical and study protocol approval from the VA Central Institutional Review
1004 Board (IRB) in accordance with the principles outlined in the Declaration of Helsinki. Over 60 VA
1005 Medical Centers have participated in this study nationally. The specific design, initial
1006 demographics of the MVP have been detailed previously²⁹. Electronic health record information
1007 from the VA's Corporate Data Warehouse (CDW) was used for clinical and demographic
1008 information. For genetic analyses, DNA extracted from whole blood was genotyped in
1009 customized Affymetrix Axiom Array which contains a total of 723,305 SNPs enriched for: 1) low
1010 frequency variants in AA and HISP populations, and 2) variants associated with diseases

1011 common to the VA population²⁹. Further quality control procedures have been previously
1012 described¹¹³.

1013 Proxy NAFLD Phenotype: MVP NAFLD phenotype definitions were developed by combining a
1014 previously published VA CDW ALT-based approach with non-invasive clinical parameters
1015 available to practicing clinicians at the point of care^{21,31}. The primary NAFLD phenotype
1016 (labeled “ALT-threshold”) was defined by: (i) elevated ALT >40 U/L for men or >30 U/L for
1017 women during at least two time points at least 6 months apart within a two-year window
1018 period at any point prior to enrollment and (ii) exclusion of other causes of liver disease (e.g.,
1019 presence of chronic viral hepatitis B or C (defined as positive hepatitis C RNA > 0 international
1020 units/mL or positive hepatitis B surface antigen), chronic liver diseases or systemic conditions
1021 (e.g., hemochromatosis, primary biliary cholangitis, primary sclerosing cholangitis, autoimmune
1022 hepatitis, alpha-1-antitrypsin deficiency, sarcoidosis, metastatic liver cancer, secondary biliary
1023 cirrhosis, Wilson’s disease), and/or alcohol use disorder (e.g., alcohol use disorder, alcoholic
1024 liver disease, alcoholic hepatitis and/or ascites, alcoholic fibrosis and sclerosis of liver, alcoholic
1025 cirrhosis of liver and/or ascites, alcoholic hepatic failure and/or coma, and unspecified alcoholic
1026 liver disease). The control group was defined by having a: normal ALT (≤ 30 U/L for men, ≤ 20 U/L
1027 for women) and no apparent causes of liver disease or alcohol use disorder or related
1028 conditions²¹. Habitual alcohol consumption was assessed with the age-adjusted Alcohol Use
1029 Disorders Identification Test (AUDIT-C) score, a validated questionnaire annually administered
1030 by VA primary care practitioners and used previously in MVP^{114,115}. Demographics of the NAFLD
1031 cohort are shown in **Supplementary Table 1**.

1032

1033

1034 *Single-variant autosomal analyses.*

1035 We tested imputed SNPs that passed quality control (i.e. HWE $> 1 \times 10^{-10}$, INFO > 0.3 , call rate $>$
1036 0.975) for association with NAFLD through logistic regression assuming an additive model of
1037 variants with MAF $> 0.1\%$ in European American (EA), and MAF $> 1\%$ in African Americans (AA),
1038 Hispanics (HISP), and Asians (ASN) using PLINK2a software¹¹⁶. Indels were excluded from
1039 analysis. Covariates included age, gender, age-adjusted AUDIT-C score, and first 10 principal
1040 components (PC's) of genetic ancestry. We aggregated association summary statistics from the
1041 ancestry-specific analyses and performed a trans-ancestry meta-analysis. The association
1042 summary statistics for each analysis were meta-analyzed in a fixed-effects model using METAL
1043 with inverse-variance weighting of log odds ratios¹¹⁷. Variants were clumped using a range of
1044 500kb and/or CEU r^2 LD > 0.05 , and were considered genome-wide significant if they passed the
1045 conventional p-value threshold of 5×10^{-8} . Trans-ancestry and ancestry-specific summary
1046 statistics are displayed in **Supplementary Tables 2-5**.

1047

1048 *Secondary signal analysis.*

1049 The PLINK --condition and --condition-list parameters were used to conduct stepwise
1050 conditional analyses on individual level data in MVP to detect ancestry-specific distinct
1051 association signals nearby lead SNPs. Regional SNPs were eligible if they were located within
1052 500kb of lead SNP, had a MAF $> 1\%$ and passed standard quality control criteria (INFO > 0.3 ,
1053 HWE $P > 1.0 \times 10^{-10}$, call rate > 0.975). Logistic regression was performed in a stepwise fashion,
1054 starting with a regional association analysis with the following set of covariates: lead SNP
1055 imputed allele dosage, age, gender, and 10 PC's of genetic ancestry. If the corresponding

1056 output file contained SNP(s) that reached locus-wide significance ($P < 1.0 \times 10^{-5}$), the most
1057 significant SNP was selected and added to the covariate set. The regression was repeated until
1058 no locus-wide significant SNPs remained. Secondary signals are shown in **Supplementary Table**
1059 **11**.

1060

1061 *Credible Sets.*

1062 We calculated Wakefield's approximate Bayes' factors⁴¹ based on the marginal summary
1063 statistics of the trans-ancestry meta-analysis and ancestry specific summary statistics using the
1064 CRAN R package *corrcoverage*¹¹⁸. For each locus, the posterior probabilities of each variant
1065 being causal were calculated and a 95% credible set was generated which contains the
1066 minimum set of variants that jointly have at least 95% posterior probability (PP) of including the
1067 causal variant (**Supplementary Tables 12-15**).

1068

1069 *External validation in a Liver Imaging cohort.*

1070 A replication lookup of lead loci was performed to evaluate the extent to which genetic
1071 predictors of hepatocellular injury (cALT) correspond with quantitative hepatic fat derived from
1072 computed tomography (CT) / magnetic resonance imaging (MRI)-measured hepatic fat in the
1073 Penn Medicine Biobank (PMBB), UK Biobank, Multi-Ethnic Study of Atherosclerosis (MESA),
1074 Framingham Heart Study (FHS), and University of Maryland Older Order Amish study
1075 (**Supplementary Table 8**). Attenuation was measured in Hounsfield units. The difference
1076 between the spleen and liver attenuation was measured for PMBB; a ratio between liver
1077 attenuation/spleen attenuation was used for MESA and Amish; and liver attenuation/phantom

1078 attenuation ratio in FHS as previously described by Speliotes *et al*¹². Abdominal MRI data from
1079 UK Biobank data were used to quantify liver fat using a two-stage machine learning approach
1080 with deep convolutional neural networks¹¹⁹. CT-measured hepatic fat was estimated using a
1081 multi-stage series of neural networks for presence of scan contrast and liver segmentation
1082 using convolutional neural networks. The PMBB included CT data on 2,979 EA and 1,250 AA
1083 participants¹²⁰, the FHS included a total of 3,011 EA participants, the Amish study 754 EA
1084 participants, and MESA contributed 1,525 EA, 1,048 AA, 923 HISP, and 360 ASN participants for
1085 concordance analysis. The UK Biobank included MRI image data from 36,703 EA participants. All
1086 cohorts underwent individual-level linear regression analysis on hepatic fat, adjusted for the
1087 covariates of age, gender, first 10 principal components of genetic ancestry, and alcohol intake
1088 if available. If the lead SNP was not available in any of the studies, a proxy SNP in high LD with
1089 the lead variant was used ($r^2 > 0.7$) or if no such variant was identified, the SNP was set to
1090 missing for that respective study. The study-specific ancestry-stratified summary statistics were
1091 first standardized to generate standard scores or normal deviates (z-scores), and then meta-
1092 analyzed using METAL in a fixed-effects model with inverse-variance weighting of regression
1093 coefficients¹¹⁷. In a first round of meta-analysis, ancestry-specific summary statistics were
1094 generated, which then served as input for a subsequent round of meta-analysis that represents
1095 the trans-ancestry effects of our lead SNPs on quantitative hepatic fat.

1096

1097 *External validation in a Liver Biopsy cohort*

1098 Available data from the following groups contributed to the Liver Biopsy Cohort.

1099 Non-Alcoholic Steatohepatitis Clinical Research Network (NASH CRN) studies with Hispanic
1100 Boys, FLINT, PIVENS and NASH Women Studies: Results from several studies of EA and HISP
1101 participants were included from the Lundquist Institute. The Hispanic cases are derived from
1102 the NAFLD Pediatric Database I (NAFLD Peds DB1), a prospective, longitudinal, multicenter,
1103 observational study cohort of adults and children initiated in 2002 and contains over 4,400
1104 subjects¹²¹. Clinical and histologic features of database participants have been described by
1105 Patton et al¹²². Biopsy specimens were reviewed and scored centrally by the Non-Alcoholic
1106 Steatohepatitis Clinical Research Network (NASH CRN) Pathology Committee according to the
1107 histology scoring system established by the NASH CRN¹²³. Genotyping was performed using the
1108 Illumina HumanCNV370-Quadv3 BeadChip at the Medical Genetics Institute at Cedars–Sinai
1109 Medical Center (HumanCNV370-Quadv3 BeadChips; Illumina, San Diego, CA, USA). The Hispanic
1110 controls from NASH CRN are derived from the Long QT Screening (LQTS) study¹²⁴. Saliva
1111 samples were used for genotyping with the Illumina HumanCore-24 BeadChips at the Institute
1112 for Translational Genomics and Population Sciences of the Lundquist Institute at Harbor-UCLA
1113 Medical Center. For all Hispanic samples, SNP data were imputed to the 1000 Genomes Project
1114 phase 3 dataset version 5 (AMR population) on the Michigan imputation server. The final
1115 dataset consisted of 787 samples, including 208 cases from NASH Boys and 579 controls from
1116 LQTS, and the top 3 PCs were included in the association analysis.

1117 The European American NAFLD samples from Lundquist Institute are derived from
1118 FLINT, PIVENS, and NASH women studies, and the controls are derived from the Cholesterol
1119 and Atherosclerosis Pharmacogenetics (CAP) trial. The details of the FLINT study have been
1120 published previously¹²⁵. Liver histology was blindly and centrally assessed by the NASH Clinical

1121 Research Network (NASH CRN) Pathology Committee according the NASH CRN system¹²³. A
1122 total of 244 patients with available DNA were genotyped of whom 198 (81%) were White¹²⁶.
1123 Genotyping was performed using the Omni2.5 content GWAS chip. The PIVENS study, a study of
1124 Pioglitazone versus Vitamin E versus Placebo in non-diabetic adults has been described
1125 previously⁶⁹. Genotyping was performed on 432 PIVENS samples along with the FLINT samples
1126 using the Omni2.5 content GWAS chip. Subjects were removed for failed genotyping,
1127 unresolvable gender discrepancies, being outliers by principal component analyses, and by
1128 relatedness. In total, 197 White samples remained in the analysis dataset. The NASH Women
1129 study included a subset of patients who were into the NAFLD Database Study of NASH CRN
1130 whose liver biopsy specimens were reviewed and scored centrally by the NASH CRN Pathology
1131 Subcommittee. For the GWAS ancillary study²² genotyping was performed at the Medical
1132 Genetics Institute at Cedars–Sinai Medical Center with the use of Infinium HD technology
1133 (HumanCNV370-Quadv3 BeadChips; Illumina, San Diego, CA). The controls for the European
1134 American analysis from Lundquist Institute are derived from the CAP trial involved 944 healthy
1135 volunteers, 609 of whom were Caucasian¹²⁷. In total, 591 subjects were genotyped on the
1136 Illumina HumanHap300 BeadChip or Illumina HumanCNV610-Quad beadchip. Imputation was
1137 performed using the Michigan Imputation Server with the reference panel of the Haplotype
1138 Reference Consortium (HRC) 1.1 release in 2016. After final QC of European American cohorts,
1139 the final 1,225 samples in the analysis including 650 cases and 575 controls, and the top 3 PCs
1140 for genetic ancestry were included in the association analysis. The NASH CRN database and
1141 clinical trials were reviewed and approved by the individual institutional review boards at each
1142 participating site. All participants signed an informed consent prior to their enrollment into

1143 these consents and their de-identified genetic data to be used for future liver disease research
1144 by the NASH CRN investigators and by their collaborators. These studies have been monitored
1145 by an NIDDK-sponsored data safety and monitoring board.

1146

1147 EPOS Consortium Cohort: Results from EPOS consortium cohort were included from Newcastle
1148 University. A total 1,483 histologically characterized NAFLD cases were included and 17,781
1149 genetically matched controls, with the cases recruited into the European NAFLD Registry
1150 (ClinicalTrials.gov Identifier: NCT04442334) from clinics at several leading European tertiary
1151 liver centres²⁰. Details of inclusion/exclusion criteria have previously been described^{20,128}. All
1152 patients had undergone liver biopsy as part of the routine diagnostic workup for presumed
1153 NAFLD, and routinely assessed according to accepted criteria by experienced liver pathologists
1154 and scored using the well validated NIDDK NASH CRN system¹²³. Genotyping was performed
1155 using the Illumina OmniExpress BeadChip by Edinburgh Clinical Research Centre. The 17,781
1156 population controls were recruited from existing genome-wide genotype data: Wellcome Trust
1157 Case Control Consortium, (n=5,159) typed on the Illumina Human1.2M-Duo; the Hypergenes
1158 cohort (n=1,520) typed on the Illumina Human1M-Duo, KORA (n=1,835) genotyped on the
1159 Illumina HumanOmni2.5 Exome chip, and Understanding Societies (n=9,267) typed on the
1160 Illumina HumanCoreExome chip. Overlapping SNPs that were well genotyped in all case and
1161 control cohorts were imputed together to the Haplotype Resource Consortium panel (HRC 1.1r
1162 2016) by the Michigan Imputation Server.

1163 The Geisinger Health System (GHS) bariatric surgery cohort: This consisted of 3,599 individuals
1164 of European descent. Wedge biopsies of the liver were obtained intraoperatively during

1165 bariatric surgery, and liver histology was conducted by an experienced pathologist and
1166 subsequently re-reviewed by a second experienced pathologist using the NASH CRN scoring
1167 system¹²³. A total of 806 participants did not have NAFLD and were classified as controls,
1168 whereas 2,793 were histologically characterized as having NAFLD. DNA sample preparation and
1169 whole-exome sequencing were performed at the Regeneron Genetics Centre¹²⁹. Exome capture
1170 was performed using NimbleGen probes according to the manufacturer's recommended
1171 protocol (Roche NimbleGen) multiplexed samples were sequenced on an Illumina v4 HiSeq
1172 2500. Raw sequence data from each run were uploaded to the DNAnexus platform for
1173 sequence read alignment and variant identification.

1174 STELLAR-3 and ATLAS studies: Results from two trials from Gilead Sciences were included
1175 including phase 3 STELLAR-3 study (ClinicalTrials.gov Identifier: NCT03053050), and phase 2
1176 ATLAS study (ClinicalTrials.gov Identifier: NCT03449446) which were
1177 discontinued/terminated¹³⁰. Genotyping was performed using whole genome sequencing
1178 (Illumina) aimed at 100x coverage. The PyVCF script was used to extract allele frequencies from
1179 VCF files generated using GATK4 pipeline with hg38 as reference genome.

1180 BioVU Biorepository: BioVU subjects at Vanderbilt University underwent SNP genotyping using
1181 the Illumina Infinium Multi-Ethnic Genotyping Array (MEGAEX) platform and underwent QC
1182 analyses and imputation as previously described¹³¹. Genetic data for were imputed using the
1183 Michigan Imputation Server (HRC v1.1) and genotyping data was linked to de-identified EHR
1184 data. All available lab measurements in this cohort that occurred when the subject was at least
1185 18 years of age. BioVU participants were selected based on available pathology report for liver
1186 biopsy in the note table in Observational Medical Outcomes Partnership (OMOP), excluding

1187 those with other conflicting diagnoses (e.g. viral hepatitis, alcohol, transplant, explant). NAFLD
1188 was defined based on pathology report defining hepatic fat as mild, moderate, severe, 5% or
1189 more.

1190

1191 Control subjects within BloVU were identified by selecting those with ALT levels below 30 for
1192 males and below 20 for females. Both cases and controls were excluded for alcohol use
1193 disorders using ICD-9 and -10 codes.

1194

1195 Penn Medicine Biobank (PMBB): The Penn Medicine Biobank includes participants recruited
1196 from the University of Pennsylvania Health System. A total of 139 biopsy proven NAFLD cases
1197 were selected using Linguamatics natural language processing on biopsy protocols of the PENN
1198 EHR. Cases were then linked to the PennMedicine BioBank. In addition, 1,995 PMBB
1199 participants were classified as controls if a recent CT scan of the liver was available, but no
1200 steatosis was present. Appropriate consent was obtained from each participant regarding
1201 storage of biological specimens, genetic sequencing, and access to all available EHR data. DNA
1202 extracted from the blood plasma of 2,134 samples were genotyped in three batches: the
1203 Illumina QuadOmni chip at the Regeneron Genetics Center; the Illumina GSA V1 chip OR on the
1204 Illumina GSA V2 chip by the Center for Applied Genomics at the Children's Hospital of
1205 Philadelphia. Genotypes for each of the three PMBB datasets were imputed to the 1000
1206 Genomes reference panel (1000G Phase3 v5) using the Michigan Imputation Server. Results
1207 from liver biopsy data are shown in **Supplemental Tables 6 and 7**.

1208

1209 *Heritability estimates and genetic correlations analysis.*

1210 LD-score regression was used to estimate the heritability coefficient, and subsequently
1211 population and sample prevalence estimates were applied to estimate heritability on the
1212 liability scale¹³². A genome-wide genetic correlation analysis was performed to investigate
1213 possible co-regulation or a shared genetic basis between cALT and other complex traits and
1214 diseases (**Supplementary Table 10**). Pairwise genetic correlation coefficients were estimated
1215 between the meta-analyzed NAFLD GWAS summary output in EA and each of 774 precomputed
1216 and publicly available GWAS summary statistics for complex traits and diseases by using LD
1217 score regression through LD Hub v1.9.3 (<http://ldsc.broadinstitute.org>). Statistical significance
1218 was set to a Bonferroni-corrected level of $P < 6.5 \times 10^{-5}$.

1219

1220 *Tissue- and epigenetic-specific enrichment of NAFLD heritability.*

1221 We analyzed cell type-specific annotations to identify enrichments of NAFLD heritability as
1222 shown in **Supplementary Table 16**. First, a baseline gene model was generated consisting of 53
1223 functional categories, including UCSC gene models, ENCODE functional annotations¹³³,
1224 Roadmap epigenomic annotations¹³⁴, and FANTOM5 enhancers¹³⁵. Gene expression and
1225 chromatin data were also analyzed to identify disease-relevant tissues, cell types, and tissue-
1226 specific epigenetic annotations. We used LDSC³⁷⁻³⁹ to test for enriched heritability in regions
1227 surrounding genes with the highest tissue-specific expression. Sources of data that were
1228 analyzed included 53 human tissue or cell type RNA-seq data from GTEx²⁸; human, mouse, or
1229 rat tissue or cell type array data from the Franke lab¹³⁶; 3 sets of mouse brain cell type array
1230 data from Cahoy *et al*¹³⁷; 292 mouse immune cell type array data from ImmGen¹³⁸; and 396

1231 human epigenetic annotations from the Roadmap Epigenomics Consortium¹³⁴. Expression
1232 profiles are considered statistically significantly enriched for T2D susceptibility if they pass the
1233 nominal P-value threshold of 0.001.

1234

1235 *Pathway Annotation enrichment.*

1236 Enrichment analyses in DEPICT¹³⁹ were conducted using genome-wide significant ($P < 5 \times 10^{-8}$)
1237 NAFLD GWAS lead SNPs (**Supplementary Table 18**). DEPICT is based on predefined phenotypic
1238 gene sets from multiple databases and Affymetrix HGU133a2.0 expression microarray data
1239 from >37k subjects to build highly-expressed gene sets for Medical Subject Heading (MeSH)
1240 tissue and cell type annotations. Output includes a P-value for enrichment and a yes/no
1241 indicator of whether the FDR q-value is significant ($P < 0.05$). Tissue and gene-set enrichment
1242 features are considered. We tested for epigenomic enrichment of genetic variants using
1243 GREGOR software (**Supplementary Table 19**)¹⁴⁰. We selected EA-specific NAFLD lead variants
1244 with a p-value less than 5×10^{-8} . We tested for enrichment of the resulting GWAS lead variants
1245 or their LD proxies (r^2 threshold of 0.8 within 1 Mb of the GWAS lead, 1000 Genomes Phase I) in
1246 genomic features including ENCODE, Epigenome Roadmap, and manually curated data
1247 (**Supplemental Table 20**). Enrichment was considered significant if the enrichment p-value was
1248 less than the Bonferroni-corrected threshold of $P = 1.8 \times 10^{-5}$ ($0.05 / 2,725$ tested features).

1249

1250 *Coding variant mapping.*

1251 All imputed variants in MVP were evaluated with Ensemble variant effect predictor¹⁴¹, and all
1252 predicted LoF and missense variants were extracted. The LD was calculated with established

1253 variants for trans-ancestry, EA, AA, and HISP lead SNPs based on 1000 Genomes reference
1254 panel¹⁴². For SNPs with low allele frequencies, the MVP dataset was used for LD calculation for
1255 the respective underlying population. For the trans-ancestry coding variants, the EA panel was
1256 used for LD calculation. Coding variants that were in strong LD ($r^2 > 0.7$) with lead SNPs and had
1257 a strong statistical association ($P\text{-value} < 1 \times 10^{-5}$) were considered the putative causal drivers of
1258 the observed association at the respective locus (**Supplementary Table 22**).

1259

1260

1261

1262 *Colocalization with gene expression*

1263 GWAS summary statistics were lifted over from GRCh37 to GRCh38 using LiftOver
1264 (<https://genome.ucsc.edu/cgi-bin/hgLiftOver>). Colocalization analysis was run separately for
1265 eQTLs and sQTLs for each of the 49 tissues in GTEx v8 (**Supplementary Tables 23 and 24**)²⁸. For
1266 each tissue, we obtained an LD block for the genome with a sentinel SNP at $P < 5 \times 10^{-8}$, and then
1267 restricted analysis to the LD blocks. For each LD block with a sentinel SNP, all genes within 1Mb
1268 of the sentinel SNP (cis-Genes) were identified, and then restricted to those that were
1269 identified as eGenes in GTEx v8 at an FDR threshold of 0.05 (cis-eGenes). For each cis-eGene,
1270 we performed colocalization using all variants within 1Mb of the gene using the default prior
1271 probabilities in the 'coloc' function for the coloc package in R. We first assessed each coloc
1272 result for whether there was sufficient power to test for colocalization ($PP3+PP4>0.8$), and for
1273 the colocalization pairs that pass the power threshold, we defined the significant colocalization
1274 threshold as $PP4/(PP3+PP4)>0.9$.

1275

1276 *Overlap with open chromatin.*

1277 At each of the 77 NAFLD-associated loci from the trans-ancestry meta-analysis, we looked for
1278 overlaps between any variant in the credible set, and regions of open chromatin previously
1279 identified using ATAC-Seq experiments in two cell types—3 biological replicates of HepG2¹⁴³
1280 and 3 biological replicates of hepatocyte-like cells (HLC)¹⁴⁴ produced by differentiating three
1281 biological replicates of iPSCs, which in turn were generated from peripheral blood mononuclear
1282 cells using a previously published protocol⁴⁴. Results are shown in **Supplementary Table 25**.

1283

1284 *Overlap with Promoter Capture-C data.*

1285 We used two promoter Capture-C datasets from two cell/tissue types to capture physical
1286 interactions between gene promoters and their regulatory elements and genes; three biological
1287 replicates of HepG2 liver carcinoma cells, and hepatocyte-like cells (HLC)¹⁴³. The detailed
1288 protocol to prepare HepG2 or HLC cells for the promoter Capture-C experiment is previously
1289 described⁴⁴. Briefly, for each dataset, 10 million cells were used for promoter Capture-C library
1290 generation. Custom capture baits were designed using an Agilent SureSelect library design
1291 targeting both ends of DpnII restriction fragments encompassing promoters (including
1292 alternative promoters) of all human coding genes, noncoding RNA, antisense RNA, snRNA,
1293 miRNA, snoRNA, and lincRNA transcripts, totaling 36,691 RNA baited fragments. Each library
1294 was then sequenced on an Illumina NovoSeq (HLC), or Illumina HiSeq 4000 (HLC), generating
1295 1.6 billion read pairs per sample (50 base pair read length.) HiCUP¹⁴⁵ was used to process the
1296 raw FastQ files into loop calls; we then used CHiCAGO¹⁴⁶ to define significant looping

1297 interactions; a default score of 5 was defined as significant. We identified those NAFLD loci at
1298 which at least one variant in the credible set interacted with an annotated bait in the Capture-C
1299 data (**Supplementary Table 25**).

1300

1301 *Protein-Protein Interaction Network Analysis*

1302 We employed the search tool for retrieval of interacting genes (STRING) v11¹⁴⁷ ([https://string-](https://string-db.org)
1303 [db.org](https://string-db.org)) to seek potential interactions between nominated genes. STRING integrates both
1304 known and predicted PPIs and can be applied to predict functional interactions of proteins. In
1305 our study, the sources for interaction were restricted to the ‘Homo Sapiens’ species and limited
1306 to experimentally validated and curated databases. An interaction score ≥ 0.4 were applied to
1307 construct the PPI networks, in which the nodes correspond to the proteins and the edges
1308 represent the interactions (**Figure 4, Supplemental Table 26**).

1309

1310 *Ensemble variant-to-gene mapping to identify putative causal genes.*

1311 Based on DEPICT gene prediction, coding variant linkage analysis, QTL analysis, and annotation
1312 enrichment, and PPI networks (**Supplemental Tables 18-26**), a total of 215 potentially relevant
1313 genes for NAFLD were mapped to trans-ancestry 77 loci. For each locus, we counted how many
1314 times each gene in that region was identified in the 8 analyses. We then divided this number by
1315 the total number of experiments (i.e., 8) to calculate an evidence burden (called nomination
1316 score) that ranges from 0 to 100%. For each genomic locus, the gene that was most frequently
1317 identified as a causal gene was selected as the putative causal gene for that locus. In the case of
1318 a tie break, and if the respective genes have identical nomination profiles, the gene with eQTLs

1319 in multiple tissues was selected as the putative causal gene. Similarly, gene nomination was
1320 preferred for loci that strongly tagged ($r^2 > 0.8$) a coding variant. Loci that scored with 3 distinct
1321 sources of evidence or greater are listed for coding variant (**Table 1A**) and non-coding variants
1322 (**Table 1B**), respectively.

1323

1324 *MVP LabWAS.*

1325 A total of 21 continuous traits in the discovery MVP dataset, e.g. AST, ALP, fasting TG, HDL, LDL,
1326 TC, random glucose, HbA1c, albumin, bilirubin, platelet count, BMI, blood urea nitrogen (BUN),
1327 creatinine, eGFR, SBP, DBP, ESR, INR, and C-reactive protein were tested in 186,681 EA's with
1328 association of 77 SNPs using linear regression of log-linear values. Covariates included age,
1329 gender and the first 10 PC's of EA ancestry (**Supplementary Table 29**). The Bonferonni p-value
1330 threshold is set at 3.09×10^{-05} ($0.05 / 21 \text{ traits} * 77 \text{ SNPs}$)

1331

1332 *PheWAS with UK Biobank data.*

1333 For the 77 lead trans-ancestry SNPs and EA and AA specific SNPs, we performed a PheWAS in a
1334 genome-wide association study of EHR-derived ICD billing codes from the White British
1335 participants of the UK Biobank using PheWeb¹⁴⁸. In short, phenotypes were classified into 1,403
1336 PheWAS codes excluding SNP-PheWAS code association pairs with case counts less than fifty¹⁴⁹.
1337 All individuals were imputed using the Haplotype Reference Consortium panel¹⁵⁰, resulting in
1338 the availability of 28 million genetic variants for a total of 408,961 subjects. Analyses on binary
1339 outcomes were conducted using a model named SAIGE, adjusted for genetic relatedness,
1340 gender, year of birth and the first 4 PC's of white British genetic ancestry¹⁵¹. SAIGE stands for

1341 Scalable and Accurate Implementation of GEneralized mixed model and represents a
1342 generalized mixed-model association test that accounts for case-control imbalance and sample
1343 relatedness¹⁵¹. Results are shown in **Supplemental Tables 30 and 31**. SNP-trait associations are
1344 listed if they passed a nominal significance threshold of $P < 0.001$, and are considered Bonferoni
1345 significant when $P < 4.6 \times 10^{-7}$ ($0.05 / 77 \text{ SNPs} * 1,403 \text{ traits}$).

1346

1347 *IEU OpenGWAS project SNP lookup.*

1348 An additional phenome-wide lookup was performed for 77 lead trans-ancestry SNPs and EA and
1349 AA specific SNPs in Bristol University's MRC Integrative Epidemiology Unit (IEU) GWAS
1350 database¹⁵². This database consists of 126,114,500,026 genetic associations from 34,494 GWAS
1351 summary datasets, including UK Biobank (<http://www.nealelab.is/uk-biobank>), FinnGen
1352 (<https://github.com/FINNGEN/pheweb>), Biobank Japan (<http://jenger.riken.jp/result>), the
1353 NHGRI-EBI GWAS catalog (<https://www.ebi.ac.uk/gwas>), a large-scale blood metabolites
1354 GWAS¹⁵³, circulating metabolites GWAS¹⁵⁴, the MR-Base manually curated database¹⁵⁵, and a
1355 protein level GWAS¹⁵⁶. Results are shown in **Supplemental Table 32**.

1356

1357 *Regional cardiometabolic cross-trait colocalization.*

1358 Bayesian colocalization tests between NAFLD-associated signals and the following trait- and
1359 disease-associated signals were performed using the COLOC R package¹⁵⁷. To enable cross-trait
1360 associations, we compiled summary statistics of 36 cardiometabolic and blood cell-related
1361 quantitative traits and disease from GWAS studies conducted in EA ancestry individuals, and for
1362 MVP-based reports also on AA and HISP. To summarize, for total, HDL, and LDL cholesterol,

1363 triglycerides, alcohol use disorder, alcohol intake, systolic blood pressure, diastolic blood
1364 pressure, type 2 diabetes, BMI, CAD, we used the summary statistics available from various
1365 MVP-based studies^{27,114,158}. Of these, the summary statistics for CAD and BMI GWAS in MVP
1366 have not been published or deposited as of yet. Data on WHR were derived from GIANT
1367 Consortium¹⁵⁹, whereas summary statistics on CKD, gout, blood urea nitrogen, urate, urinary
1368 albumin-to-creatinine ratio, microalbuminuria, and eGFR were derived from CKD Genetics
1369 Consortium¹⁶⁰⁻¹⁶². Finally, summary statistics of blood cell traits (e.g. platelet count, albumin,
1370 white blood cells, basophils, eosinophils, neutrophils, hemoglobin, hematocrit, immature
1371 reticulocyte fraction, lymphocytes, monocytes, reticulocytes, mean corpuscular hemoglobin,
1372 mean corpuscular volume, mean platelet volume, platelet distribution width, and red cell
1373 distribution width) were derived from a large-scale GWAS report performed in UK Biobank and
1374 INTERVAL studies¹⁶³. A colocalization test was performed for all 77 NAFLD loci spanning 500kb
1375 region around the lead SNP for all 36 compiled traits. For each association pair COLOC was run
1376 with default parameters and priors. COLOC computed posterior probabilities for the following
1377 five hypotheses: PP0, no association with trait 1 (cALT GWAS signal) or trait 2 (e.g., co-
1378 associated metabolic signal); PP1, association with trait 1 only (i.e., no association with trait 2);
1379 PP2, association with trait 2 only (i.e., no association with trait 1); PP3, association with trait 1
1380 and trait 2 by two independent signals; and PP4, association with trait 1 and trait 2 by shared
1381 variants. Evidence of colocalization¹⁶⁴ was defined by $PP3 + PP4 \geq 0.99$ and $PP4/PP3 \geq 5$. Results
1382 are shown in **Supplemental Table 33**.

1383

1384 *Genetic risk scores and histologically characterized NAFLD.*

1385 We constructed genetic risk scores (GRS) in 4 histologically characterized cohorts (e.g.
1386 Lundquist Whites and Hispanics, EPoS Consortium Whites, and BioVU Whites) by calculating a
1387 linear combination of weights derived from the MVP dataset of lead 77 trans-ancestry cALT
1388 variants that passed conventional genome-wide significance (GRS-77, $P < 5.0 \times 10^{-8}$). The GRS-77
1389 was standardized and the risk of histologically characterized NAFLD was assessed using a
1390 logistic regression model together with the potential confounding factors of age, gender, and
1391 the first 3 to 5 principal components of ancestry. To delineate the potential driving effects of
1392 known NAFLD loci, we divided the 77 loci into two sets, and generated one PRS consisting of 7
1393 known NAFLD SNPs only (GRS-7), and one of newly identified 70 cALT SNPs (GRS-70). The goal
1394 of this separation is to evaluate whether a GRS based on novel SNPs alone (GRS-70) showed
1395 predictive capability for biopsy-proven histologically characterized NAFLD. Both GRS's were
1396 added as independents in a logistic regression model to explain histologically characterized
1397 NAFLD with the confounders of age, gender, and PC's of ancestry. The individual effect sizes for
1398 each study were then meta-analyzed using the metagen package in R with random effects
1399 model comparing the standardized mean difference (**Supplemental Table 9**). Finally, a forest
1400 plot was created to visualize the effect estimates between the studies (**Supplemental Figure 8**).

1401

1402 *Transcription Factor Analysis.*

1403 We identified nominated genes (**Supplemental Table 28**) that encode for TFs based on known
1404 motifs, inferred motifs from similar proteins, and likely sequence specific TFs according to
1405 literature or domain structure¹⁶⁵. Target genes for these TFs were extracted using DoRoThEA
1406 database¹⁶⁶ in OmniPath collection¹⁶⁷ using the associated Bioconductor R package

1407 OmnipathR¹⁶⁸, a gene set resource containing TF-TF target interactions curated from public
1408 literature resources, such as ChIP-seq peaks, TF binding site motifs and interactions inferred
1409 directly from gene expression.

1410

1411 **Acknowledgements**

1412 This research is based on data from the Million Veteran Program, Office of Research and
1413 Development, Veterans Health Administration and was supported by award no. MVP000. This
1414 publication does not represent the views of the Department of Veterans Affairs, the US Food
1415 and Drug Administration, or the US Government. This research was also supported by funding
1416 from: the Department of Veterans Affairs awards I01- BX003362 (P.S.T. and K.M.C) and
1417 I01BX003341 (H.R.K. Co-Principal Investigator) and the VA Informatics and Computing
1418 Infrastructure (VINCI) VA HSR RES 130457 (S.L.D). B.F.V. acknowledges support for this work
1419 from the NIH/NIDDK (DK101478 and DK126194) and a Linda Pechenik Montague Investigator
1420 award. K.M.C, S.M.D, J.M.G, C.J.O, L.S.P, and P.S.T. are supported by the VA Cooperative Studies
1421 Program. S.M.D. is supported by the Veterans Administration [IK2 CX001780]. Funding support
1422 is also acknowledged for M.S. (K23 DK115897), R.M.C (R01 AA026302), D.K. (National Heart,
1423 Lung, and Blood Institute of the National Institutes of Health [T32 HL007734]), J.B.M
1424 (R01HL151855, UM1DK078616), L.S.P. (VA awards I01 CX001025, and I01 CX001737, NIH
1425 awards R21 DK099716, U01 DK091958, U01 DK098246, P30 DK111024, and R03 AI133172, and
1426 a Cystic Fibrosis Foundation award PHILLI2A0). The Rader lab was supported by NIH grants
1427 HL134853 (NJH and DJR) and DK114291-01A1 (K.T.C, N.J.H, and D.J.R). We thank all study
1428 participants for their contribution. Support for imaging studies was provided by ITMAT (NIH

1429 NCATS UL1TR001878), the Penn Center for Precision Medicine Accelerator Fund and R01
1430 HL137501. Data for external replication and hepatic fat concordance were provided by
1431 investigators using United Kingdom BioBank, Multi-Ethnic Study of Atherosclerosis (MESA), Old
1432 Order Amish Study (Amish), Framingham Heart Study (FHS) and Penn Medicine Biobank
1433 (PMBB).

1434

1435 **MESA/MESA SHARe Acknowledgements:** MESA and the MESA SHARe projects are conducted
1436 and supported by the National Heart, Lung, and Blood Institute (NHLBI) in collaboration with
1437 MESA investigators. This research was supported by R01 HL071739 and MESA was supported
1438 by contracts 75N92020D00001, HHSN268201500003I, N01-HC-95159, 75N92020D00005, N01-
1439 HC-95160, 75N92020D00002, N01-HC-95161, 75N92020D00003, N01-HC-95162,
1440 75N92020D00006, N01-HC-95163, 75N92020D00004, N01-HC-95164, 75N92020D00007, N01-
1441 HC-95165, N01-HC-95166, N01-HC-95167, N01-HC-95168, N01-HC-95169, UL1-TR-000040, UL1-
1442 TR-001079, UL1-TR-001420. Also supported in part by the National Center for Advancing
1443 Translational Sciences, CTSI grant UL1TR001881, and the National Institute of Diabetes and
1444 Digestive and Kidney Disease Diabetes Research Center (DRC) grant DK063491 to the Southern
1445 California Diabetes Endocrinology Research Center.

1446

1447 **NASH CRN Acknowledgements:** The NASH Boys study was supported by NIDDK (U01DK061734,
1448 U01DK061718, U01DK061728, U01DK061731, U01DK061732, U01DK061737, U01DK061738,
1449 U01DK061730, U01DK061713) and NICHD. It was also supported by NIH CTSA awards
1450 (UL1TR000040, UL1RR024989, UL1RR025761, M01RR00188, UL1RR024131, UL1RR025014,

1451 UL1RR031990, UL1RR025741, UL1RR029887, UL1RR24156, UL1RR025055, UL1RR031980), and
1452 DRC HDK063491. LQTS was supported by the National Institutes of Health (grant
1453 5R42HL112435-04 to QT Medical, Inc.). The provision of genotyping data was supported in part
1454 by the National Center for Advancing Translational Sciences, CTSI grant UL1TR001881, and the
1455 National Institute of Diabetes and Digestive and Kidney Disease Diabetes Research Center (DRC)
1456 grant DK063491 to the Southern California Diabetes Endocrinology Research Center. For LQTS:
1457 QT Medical, Inc., was involved in the study design and collection of data. However, QT Medical,
1458 Inc., had no involvement in the analysis and interpretation of the data, the drafting of the
1459 article, or the decision to submit the article for publication. The FLINT trial was conducted by
1460 the NASH CRN and supported in part by a Collaborative Research and Development Agreement
1461 (CRADA) between NIDDK and Intercept Pharmaceuticals. The Nonalcoholic Steatohepatitis
1462 Clinical Research Network (NASH CRN) is supported by the National Institute of Diabetes and
1463 Digestive and Kidney Diseases (NIDDK) (grants U01DK061718, U01DK061728, U01DK061731,
1464 U01DK061732, U01DK061734, U01DK061737, U01DK061738, U01DK061730, U01DK061713).
1465 Additional support is received from the National Center for Advancing Translational Sciences
1466 (NCATS) (grants UL1TR000439, UL1TR000436, UL1TR000006, UL1TR000448, UL1TR000100,
1467 UL1TR000004, UL1TR000423, UL1TR000058). The PIVENS study was supported by grants from
1468 the National Institutes of Health to the NASH Clinical Research Network (U01DK61718,
1469 U01DK61728, U01DK61731, U01DK61732, U01DK61734, U01DK61737, U01DK61738,
1470 U01DK61730, U01DK61713) and, in part, by the intramural program on the NIH, National
1471 Cancer Institute. Other grant support includes the following National Institutes of Health
1472 General Clinical Research Centers or Clinical and Translational Science Awards: UL1RR024989,

1473 UL1RR024128, M01RR000750, UL1RR024131, M01RR000827, UL1RR025014, M01RR000065.

1474 Additional funding to conduct PIVENS trial was provided by Takeda Pharmaceuticals North

1475 America, Inc. through a Cooperative Research and Development Agreement (CRADA) with the

1476 National Institutes of Health. The vitamin E softgels and matching placebo were provided by

1477 Pharmavite, LLC through a Clinical Trial Agreement with the National Institutes of Health. The

1478 NASH women study was supported by U01DK061737 and K24DK069290 (N.C.), NCRR grant

1479 M01-RR00425 to the Cedars-Sinai General Research Center Genotyping core, P30DK063491 to

1480 J.R., and R01DK079888 to M.O.G. This work is supported in part by the American

1481 Gastroenterological Association (AGA) Foundation, Sucampo, ASP Designated Research Award

1482 in Geriatric Gastroenterology, and by a T. Franklin Williams Scholarship Award; Funding

1483 provided by Atlantic Philanthropies, Inc, the John A. Hartford Foundation, the Association of

1484 Specialty Professors, and the American Gastroenterological Association to R.L. This research

1485 was funded in part with the support of the UCSD Digestive Diseases Research Development

1486 Center, US PHS grant DK080506.

1487 The CAP study was supported by the National Institutes of Health: grant U19 HL069757 from

1488 the National Heart, Lung, and Blood Institute; and grant UL1TR000124 from the National Center

1489 for Advancing Translational Sciences.

1490

1491 **EPoS Acknowledgements:** The EPoS genetics study and the European NAFLD Registry have

1492 been supported by the EPoS (Elucidating Pathways of Steatohepatitis) consortium funded by

1493 the European Union Horizon 2020 Framework Program of the European Union under Grant

1494 Agreement 634413, the FLIP (Fatty Liver: Inhibition of Progression) consortium funded by the

1495 (European Union FP7 under grant agreement 241762), the LITMUS (Liver Investigation: Testing
1496 Marker Utility in Steatohepatitis) consortium funded by the European Union Innovative
1497 Medicines Initiative 2 Joint Undertaking that receives support from the European Union's
1498 Horizon 2020 research and innovation programme and EFPIA under grant agreement 777377,
1499 and the Newcastle NIHR Biomedical Research Centre.

1500

1501 **Gilead Acknowledgements:** The Stellar and Atlas were funded by Gilead Sciences, Inc.

1502

1503 **Regeneron Acknowledgements:** The Geisinger Health System bariatric-surgery biobank was
1504 funded by Regeneron Pharmaceuticals and partly supported by a grant (P30DK072488) from
1505 the Mid-Atlantic Nutrition Obesity Research Center by the National Institutes of Health (NIH).

1506

1507 **Penn Medicine Biobank Acknowledgements:** The Penn Medicine BioBank is funded by the
1508 Perelman School of Medicine at the University of Pennsylvania and by a gift from the Smilow
1509 family, and the National Center for Advancing Translational Sciences of the National Institutes
1510 of Health under CTSA Award Number UL1TR001878."

1511

1512 **BioVU Acknowledgements:** The Vanderbilt University Medical Center's BioVU projects are
1513 supported by institutional funding, private agencies, and federal grants, which include the NIH
1514 funded Shared Instrumentation Grant S10OD017985 and S10RR025141; CTSA grants
1515 UL1TR002243, UL1TR000445, and UL1RR024975; and investigator-led projects U01HG004798,

1516 R01NS032830, RC2GM092618, P50GM115305, U01HG006378, U19HL065962, R01HD074711;
1517 U01 HG004603; U01 HG006378.

1518

1519 **Ethics statement**

1520 The Central Veterans Affairs Institutional Review Board (IRB) and site-specific Research and
1521 Development Committees approved the Million Veteran Program study. All other cohorts
1522 participating in this meta-analysis have ethical approval from their local institutions. All relevant
1523 ethical regulations were followed.

1524

1525 **Data availability**

1526 The full summary level association data from the trans-ancestry, European, African American,
1527 Hispanic, and Asian meta-analysis from this report will be available through dbGAP (Accession
1528 codes will be available before publication).

1529

1530 **Disclosures**

1531 H.R.K. is a member of a Dicerna scientific advisory board; a member of the American Society of
1532 Clinical Psychopharmacology's Alcohol Clinical Trials Initiative, which during the past three
1533 years was supported by Alkermes, Amygdala Neurosciences, Arbor Pharmaceuticals, Dicerna,
1534 Ethypharm, Indivior, Lundbeck, Mitsubishi, and Otsuka; and is named as an inventor on PCT
1535 patent application #15/878,640 entitled: "Genotype-guided dosing of opioid agonists," filed
1536 January 24, 2018. D.G. is employed part-time by Novo Nordisk.